2012-12-11

A Simplified Onsite Image-Registration Approach for Radiosurgery by Partial CT

Wupeng Yin
University of Miami, kita_0303@163.com

UNIVERSITY OF MIAMI

A SIMPLIFIED ONSITE IMAGE-REGISTRATION APPROACH FOR
RADIOSURGERY BY PARTIAL CT

By

Wupeng Yin

A THESIS

Submitted to the Faculty
of the University of Miami
in partial fulfillment of the requirements for
the degree of Master of Science

Coral Gables, Florida

December 2012

UNIVERSITY OF MIAMI

A thesis submitted in partial fulfillment of
the requirements for the degree of
Master of Science

A SIMPLIFIED ONSITE IMAGE-REGISTRATION APPROACH FOR
RADIOSURGERY BY PARTIAL CT

Wupeng Yin

Approved:

_____
Weizhao Zhao, Ph.D.
Associate Professor of
Biomedical Engineering

_____
M. Brian Blake, Ph.D.
Dean of the Graduate School

_____
Jorge Bohorquez, Ph.D.
Assistant Professor of
Biomedical Engineering

_____
Xiaodong Wu, Ph.D.
CEO and President
Director of Medical Physics
Biophysics Research Institute of
America, Inc.
Lake Worth, Florida

YIN, WUPENG   (M.S., Biomedical Engineering)
<u>A Simplified Onsite Image-Registration</u>   (December 2012)
<u>Approach for Radiosurgery by Partial CT</u>

Abstract of a thesis at the University of Miami.

Thesis supervised by Professor Weizhao Zhao.
No. of pages in text. (63)

Stereotactic radiosurgery (SRS) is a kind of method of radiation therapy that uses three-dimensional computerized imaging to precisely guide a high-powered X-ray beam to deliver a concentrated dose of radiation to the abnormal area of the body. This therapy can efficiently and successfully treat many different types of tumors, either benign or malignant. Commonly used radiosurgery treatments are applied by CyberKnife or Gamma Knife through Stereotactic mechanism. Stereotactic radiosurgery can be assisted by two and three dimensional imaging during a course of radiation treatment. This is usually called Image-guided radiation therapy (IGRT), which utilizes the imaging coordinates to direct radiation beams to follow the actual radiation treatment plan.

The image-guided system is the essential item to enable superior accuracies in the dose delivery by locating the patient's instantaneous position during radiation treatments. In CyberKnife system current setup, two X-ray imaging sources and cameras are orthogonally mounted around the patient allowing instantaneous X-ray images to be obtained. This thesis presents a method that uses the technique of computed tomography, called partial CT, to guide the stereotactic surgery and significantly simplifies the image registration procedure by one set of X-ray sources and radiation detectors. The image processing for the partial CT is based on mutual information algorithm, a technically

successful method, which ensures the accuracy of the image guidance system. All the experiments are demonstrated with respect to the CyberKnife system.

The thesis includes: 1) an overview with detailed representations for stereotactic radiosurgery techniques and devices of image guidance system applying to the radiation therapy field; 2) a hypothesis of mutual-information-based method used in partial CT image registration, demonstrations of the feasibility of the proposed method as a new image guidance system by our experiments; 3) the innovative design of the robotic couch with one X-ray camera to obtain patient's partial CT image in the treatment stage and experimental results.

Acknowledgements

Though this thesis is an independent work, I would like to take this opportunity to gratefully and sincerely extend appreciation to my family, my committee members, and friends from our lab. It would have been impossible for me to finish this task without the help and support of these individuals.

I would like to thank Dr. Zhao for his guidance, understanding, patience and most importantly, his friendship during my master studies at the University of Miami. His mentorship was paramount in encouraging me to not only be an experimentalist but also to be an independent thinker. Dr. Wu, thank you for providing me with general instruction of the real CyberKnife system in medical school. I would also like to thank Dr. Bohorquez for always giving me support.

I would like to thank my friend and co-worker Mr. Zhuang Nie for his assistance and support from the beginning of my master's study and for providing much needed humor and entertainment in the lab. Although his decision to leave the United States caused a great deal of distress for me at the time, I believe that his actions will motivate and push me forward in the future. Additionally, I am very grateful for the friendship of all the members of our lab.

Finally and most importantly, I would like thank my parents who provided tuition and fee support during my entire master's study period. Without their unconditional love and support, I would not have had this life-changing opportunity to study abroad and accomplish this thesis.

Table of Contents

List of Figures

List of Tables

Chapter 1 Introduction

1.1 Stereotactic Radiosurgery

Stereotactic Radiosurgery (SRS) is a distinct discipline that utilizes externally generated ionizing radiation in certain cases to inactivate or eradicate a defined target(s) in the head or spine without the need to make an incision[1]. The concept of stereotactic radiosurgery (SRS) came into being with the coupling of stereotaxy and radiation along who advanced imaging techniques like computed tomography (CT), magnetic resonance imaging (MRI), positron emission tomography (PET) and digital subtraction imaging (DSI), in alliance with the advancements of the computer and information technology which reawakened the use of various non-invasive and more effective methods for the treatment of multiple lesions with probably increasing accuracy and efficiency [2, 3]. Stereotactic radiosurgery has been used to treat benign and malignant tumors in the brain, vascular malformations, and other brain's disorders with minimal invasiveness for more than 30 years.

In 1951 neurosurgeon Lars Leksell developed the first stereotactic radiosurgery technique at Karolinska Hospital in Stockholm, Sweden. Dr. Leksell pioneered the stereotactic head frame for use in noninvasive lesion in functional neurosurgery by attaching an orthovoltage X-ray tube to a stereotactic frame in order to produce converging beams which would intersect at the treatment target[4]. By adjusting the width of the beam to the size of the structure to be irradiated, and moving the beam guide transversely along the frame, the targeted radiation would meet at desired tissue site[5].

The first Gamma Knife device was designed in 1968 by Dr. Leksell collaborated with Borge Larson. After getting the Food and Drug Administration (FDA) approval in 1982, the 201 Co-60 source Gamma-knife was used for the first time in the United States at the University of Pittsburgh, where it proved to be a therapeutically effective and economical alternative to some conventional neurosurgery practices[6].

In recent years, medical imaging techniques have been developed to optimize and expand the uses of the gamma knife and other stereotactic devices. Computer tomography (CT) and magnetic resonance imaging (MRI) techniques have improved the quality of the image and achieved a more precise localization of tumors in the brain; positron emission tomography (PET) scans provide images that include metabolic data and functional data of more complex targets.

There are different types of stereotactic radiosurgery. Each type uses different equipment and radiation sources. Cobalt 60 systems or Gamma-knife use cobalt as a source for gamma rays, Linear accelerator (LINAC) systems and LINAC based CyberKnife systems use high-energy X-rays to treat a tumor or other lesions. Recently developed proton beam therapy is a type of particle beam radiation therapy. Rather than using rays of radiation, such as gamma rays or X-rays, particle beam therapy uses particles such as protons or neutrons [2].

SRS relies on several technologies: Three-dimensional imaging and localization techniques that determine the exact coordinates of the target within the body; Systems to immobilize and carefully position the patient and maintain the patient position during therapy by highly focused gamma-ray or X-ray beams that converge on a tumor or abnormality; Image-guided radiation therapy (IGRT) which uses medical imaging to

confirm the location of a tumor immediately before, and during the delivery of radiation. IGRT improves the precision and accuracy of the treatment[7].

1.2 Image-Guided Radiation Therapy

Image-guided radiotherapy (IGRT) is defined as frequent imaging in the treatment room that allows treatment decisions to be made on the basis of these images. IGRT makes use of many different imaging techniques, using modalities ranging from planar imaging to fluoroscopy to cone-beam CT, and following procedures as simple as using a single set-up image or as complex as intra-fraction tumor tracking[8]. The aim of the IGRT process is to improve the accuracy of the radiation position, and to reduce the exposure of healthy tissue during radiation treatments. Theoretically, "image guidance" can be performed either statically or dynamically (in real time), using imaging for monitoring and visually feeding back to the therapist the exact position of the patient's tumor while the patient is receiving radiation therapy[9].

The development of tomographic image sets providing three-dimensional information about the patient anatomy, location, and extent of disease, and the advent of three-dimensional spatial localizer/trackers has prompted the development of techniques to determine the relationship between these distinct spaces. This process is known as registration[10].

In order to be "registered", the CyberKnife system is based on delivering SRS without an invasive head frame, and uses a simple plastic head mask to keep the head from moving during treatment which can improve patient comfort. The development of frameless SRS is possible with the incorporation of image-guidance in the delivery of treatment.

1.3 Problem Statement

Radiosurgery is a common therapeutic method used to treat cancer patient. The computer-assisted, robotic arm equipped, image-guided CyberKnife system is such a radiosurgery platform. One critical setup to perform radiosurgery is that the patient's position should be the same at the planning stage and the treatment stage so that oncologist-prescribed radiation dose can be delivered accurately at the tumor. This key step is the image registration. The X-ray stereotactic imager (XSI), a commonly used image registration system in radiosurgery, uses two orthogonally projected X-ray sources located around patient to get a pair of X-ray projection images for allowing instantaneous X-ray images to be obtained. The paired X-ray images are then compared with the computer generated paired-image set from the CT data of the same patient, in the same manner but with translation and rotation variations. The translation and rotation parameters of the best matched pair in the data set indicate patient's onsite position. The XSI technique is essentially collecting 2D information, through which 3D location is determined. Based on the CT's principle, if we rotate the subject, for each rotation degree (or sub degree), we can collect sinogram data. The sinogram data contains 3D information. Our hypothesis is that 3D information recovered from sinogram data provides more registration information than 2D projection data. In addition, the sinogram data can be obtained by one set of X-ray source and detector panel. This thesis is trying answer and test the hypothesis raised here. The technique to be used is based on CT. However, since only partial data are collected, we call it partial CT in following discussions.

In this thesis, we throughout review the CyberKnife system to understand the whole operation mechanism focusing on the sections of image-guided system and current image registration method in Chapter 2; Chapter 3 explains the sinogram and back projection of pencil-beam CT scan and the principle of mutual information applying in image registration, the simulation flashes are also demonstrated in this Chapter; The experiment designs are placed in Chapter 4, which is a simulation of using partial CT to get intraoperative images locate patient's on-site position for delivering radiation beams accurately; In Chapter 5, three experiments' are listed in sequence by verifying the feasibility of mutual information method, finding the maximum mutual information value between partial CT back projection images and testing the small scanning angles of partial CT to generate sinogram and back projection images which are capable to be mapping by mutual information.

Chapter 2 Literature Review

2.1 CyberKnife: A Robotic Frameless Stereotactic Radiosurgery System

The CyberKnife radiosurgery system has been developed in recent years, as a frameless, robotic, image-guided stereotactic radiosurgery system by manipulating an X-band linear accelerator. This recent adaptation allows for a more flexible treatment both in terms of the ability to deliver the therapy without using a frame (making the experience more comfortable for the patient) as well as increasing the fractionation flexibility. In 1996, Murphy and Cox described the accuracy of the first-generation CyberKnife and found it comparable to that of existing frame-based systems[11].

The CyberKnife radiosurgery system computes the dose range and quantity by using data from the robot and camera image tracking system software, along with contributions from the assembled team's treatment planning, based on CT imaging[12]. The CyberKnife enables facile stereotactic fractionation, eases patient discomfort due to lack of stereotactic frame, and does not require anesthesia in pediatric patients which is necessary with frame-based systems [12,13].

The CyberKnife® Robotic Radiosurgery System has undergone almost twenty years of technical development from its conception to its most recent version. The CyberKnife System, as described in a series of technical papers in the late 1990s [14, 15, 16, 17, 18, 19, 20], began as a frameless alternative to existing stereotactic radiosurgery systems such as the Gamma Knife (Elekta AB, Stockholm, Sweden) and

6

conventional linear accelerators (LINACs) equipped with head frames and stereotactic beam collimators [20]. The CyberKnife radiosurgery system is taking advantage of the inherent geometrical targeting precision of the robotic system carrying a compact X-band linear accelerator and integrated with X-ray imaging system.
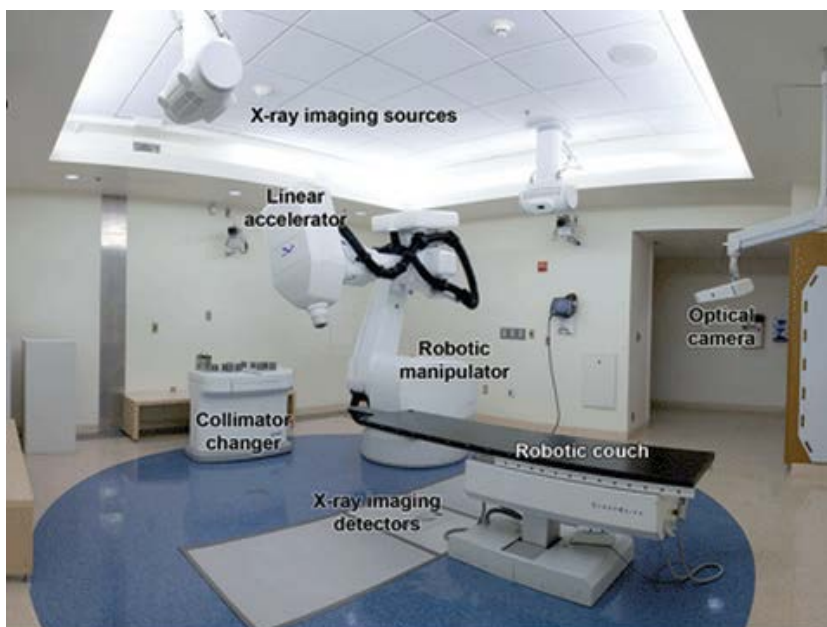
Figure 2.1: CyberKnife system includes X-ray imaging system, optical camera, linear accelerator and collimators, robotic manipulator and robotic couch.

The image-guided targeting system is composed of paired X-ray imaging sources and flat panel detectors, while the treatment delivery system is composed of a lightweight, compact 6 MV X-band LINAC, which is mounted to a robotic manipulator[21]. A pair of real-time high-resolution digital images is acquired through amorphous silicon flat panel image detectors mounted on either side of the patient. These orthogonal image pairs are registered to digitally reconstructed radiographs derived from the pretreatment CT data set by aligning implanted fiducials or bony anatomy. Differences described the spatial position (x, y, z) and the directional orientation (yaw, pitch, roll) of the target are

assessed and sent to the treatment delivery system. By using an object recognition computer algorithm and a (fiducial) marker placed within the tumor, radiation is delivered to the tumor within a predetermined margin[22]. Nowadays, this technology is using every day for treating brain [23, 24, 25, 26, 27], spine [28, 29, 30, 31, 32, 33], lung [34, 35], prostate[36], liver[37], head and neck and some extra cranial sites.

2.1.1 CyberKnife: System Hardware

LINAC Gantry: A 6MV linear accelerator mounted on a robotic manipulator with a dose-rate of 1000cGy/min.

Robotic Manipulator: The robotic manipulator is used for positioning the linear accelerator and leading the X-ray beam at the target with its six degrees of freedom around the patient.

Collimators: Collimators have been used to regular the size of radiation beam.

Robotic Couch: A five-axis table and a six-axis RoboCouch Patient Positioning System are serving together in the current CyberKnife system for adjusting patient's displacement during radiosurgery treatment. The RoboCouch table can perform automatically at all translations and rotations, the five-axis table can perform all translations but two rotations.

X-ray Stereotactic Imagers: Two diagnostic X-ray sources are mounted orthogonally to the ceiling and projecting two corresponding detector board X-ray stereotactic imagers are used for registering patient's onsite position during radiosurgery treatment.

Stereo Camera System: A stereo camera system mounted to the ceiling for measuring the position of optical markers, which are attached to the patient during the radiosurgery treatment.

2.1.2 CyberKnife: System Software

Fiducial Tracking: Fiducial markers can be used for soft tissues which are not relative to the skull or spine by imbedding the gold seeds. High intensities corresponding to these fiducial markers are displayed in the DRR images and the X-ray images during the treatment. Image-registration is based on alignment of these markers' positions between treatment stage and planning stage.

6D Skull Tracking: 6D skull tracking id normally used for intracranial lesion by using high contrast bone information.

Synchrony Tracking: Synchrony is an automated lesion tracking system. This tracking system helps changing radiation beam's position by tracking external or internal markers during the radiosurgery treatment.

Xsight Spine Tracking: Xsight spine tracking can be used for targets in the spine or near the spine.

Xsight Lung Tracking: Xsight lung tracking can be used for tracking tumors in the lung without fiducial markers.

2.2 2D/3D Image Registration in Robotic Stereotactic Radiosurgery

Recently, 2D/3D image registration is getting more and more attention because of the development of computer-assisted surgery (CAS). These CAS systems need to match preoperative images and plans to the intraoperative situation, to determine the relative

position of surgical tools and anatomy, and to accurately position and move surgical robots[38].

Several different types of 2D/3D image registration methods used in CAS system to help measuring the alignment between DRR images and X-ray images. Common registration methods can be divided into two categories: feature-based method and intensity-based method and gradient-based method. We are going to review some methods belong to feature-based registration and intensity-based registration.

Feature-based 2D/3D image registration method relies on the identifications of skull or fiducial markers to determine the alignment. Usually, the features are significant regions, lines or curves. These features should be satisfied the following qualities: they are distinctive in two stage images; they are easy to find out; they are stable during the treatment.

Intensity-based 2D/3D image registration method relies on the pixel or voxel intensity. This technique uses metrics of cross correlation, mutual information and pattern intensity. As we explained above, DRRs are created from the CT data and then used in registration with the X-ray images. The representative registration method is Normalized Cross Correlation[39]. Another significant method that comes from the information theory is the mutual information measurement. For the computation of mutual information the 2D entropy has to be computed. Maximizing the mutual information is equivalent to minimizing the spreading of the joint histogram. The method of pattern intensity measurement is introduced as "a pixel belongs to a structure if it has a significantly different intensity value from its neighboring pixels"[40].

Chapter 3 Background of Image-Guided System in CyberKnife

3.1 CT scan and Digitally Reconstructed Radiographs

IGRT makes use of many different imaging techniques, using modalities ranging from planar imaging to fluoroscopy to cone-beam CT [8]. CT can fully describe a volume of tissue by producing closely spaced axial slices of patient anatomy. As we introduced in Chapter 2, the orthogonal-intraoperative-image pairs are acquired to register to digitally reconstructed radiographs (DDR) derived from the pretreatment CT data set by aligning implanted fiducials or bony anatomy. A digitally reconstructed radiograph (DRR) is the artificial version of an X-ray image[41]. DRR images are rendered from CT volumetric data by summing the attenuation of each voxel along known ray paths through the CT volume[42].

Before starting doing applications based on a partial CT design, the principles of regular pencil-beam CT reconstruction are necessary to be reviewed here. All the sinograms and reconstruction images are created by programming pencil-beam algorithm for convenience in the following experiments of this thesis.

3.1.1 Pencil-Beam CT Scan

The development of the first modern CT scanner was begun in 1967 by Godfrey Hounsfield, an engineer at British EMI Corp[43]. In the first generation of CT scanner, a single X-ray source and a single detector cell are paired to collect all the data for a single slice. The source and detector move synchronously while the pencil beam is penetrated across the target to obtain a set of parallel sinogram at one angle. The source/detector pair

11

is then rotated to another angle and a subsequent set of measurements are obtained during a translation past the patient. This process is repeated once for all projection angles[44].
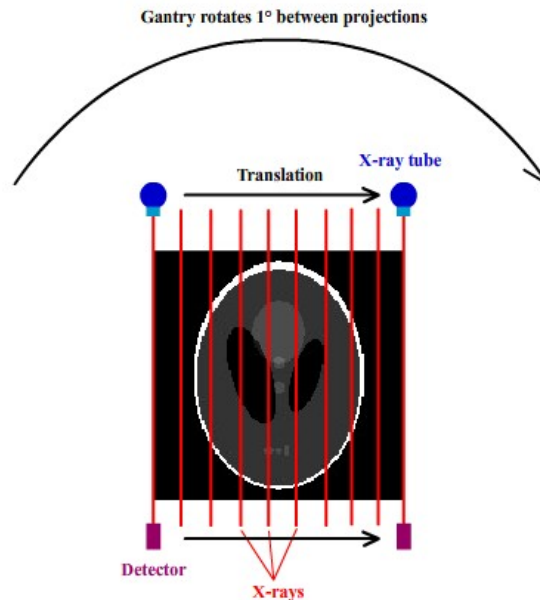
Figure 3.1: Pencil-beam CT scan. The X-ray beam penetrates the target with the opposite detector measuring the transmitted beam intensity. After one parallel scanning procedure, the X-ray tube and detector rotates to another angle.

3.1.2 Animations of the Processes of CT Scan Projection and Back Projection

Application Animation Interface: Macromedia Flash 8.0.

Adobe Flash Professional software is a useful environment for creating animation and multimedia. Flash manipulates vector and raster graphics to provide animation of text, drawings, and images, and contains an object-oriented language called ActionScript for supporting automation by the language called JavaScript Flash language (JSFL).

Flash content may be displayed on various computer systems and devices. We can using Adobe Flash Player to open the flash files.
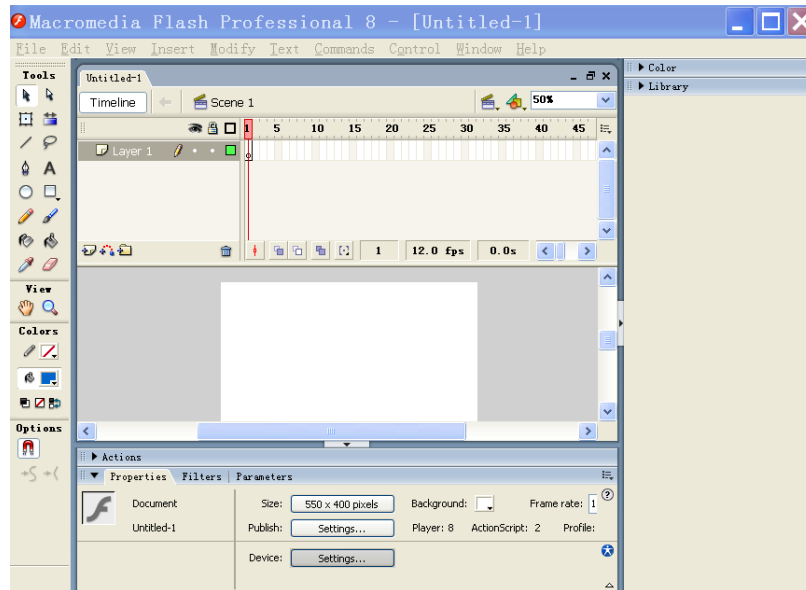
Figure 3.2: Flash creative interface. It is a multimedia platform used to add animation, video, and interactivity to web pages.

Pencil-beam CT Scan Projection

A line integral, as the name implies, represents the integral of parameters of the object along a line. In figure 3.3, object is modeled as a two-dimensional distribution of the X-ray attenuation constant and a line integral represents the total attenuation suffered by a beam of X-rays as it travels in a straight line through the object[45].

We use the system coordinates and polar coordinates to describe line integrals and projections. In this example the object is represented by a two-dimensional function $f(x, y)$ and each line integral by the (R, θ) parameters.
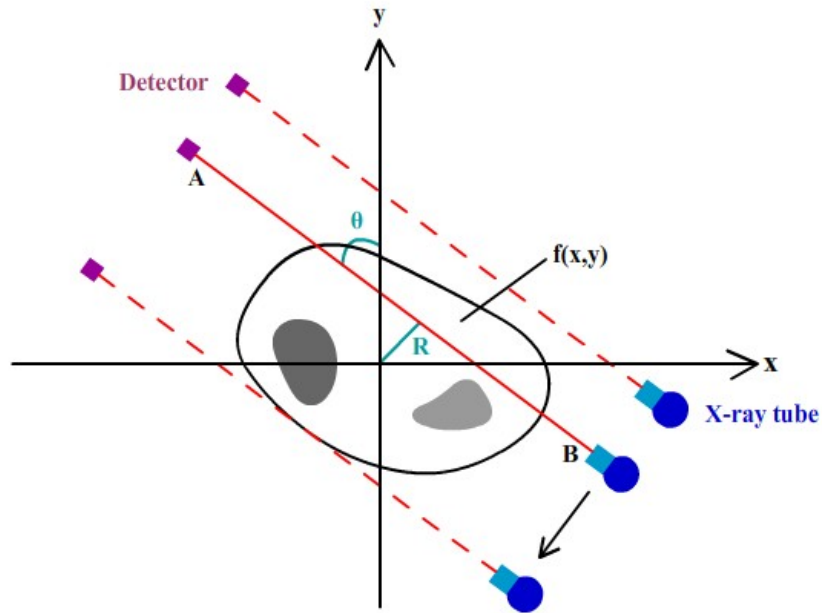
Figure 3.3: Human section under measuring and X-ray path coordinate.

The equation of line AB in Figure 3.3 is:

$$x \cos \theta + y \sin \theta = R \qquad\qquad (Eq.\,1)$$

To define line integral P_θ (R, θ) as:

$$P_\theta(R, \theta) = \int_{(R,\theta)line} F(x, y) ds \qquad\qquad (Eq.\,2)$$

. Equation 2 can be rewritten by using a delta function:

$$P_\theta(R, \theta) = \iint f(x, y) \delta(x \cos \theta + y \sin \theta - R)\, dx\, dy \qquad (Eq.\,3)$$

The function P_θ (R, θ) is known as the Radon transform of the function f(x, y).

The following figure shows the pencil-beam CT projection procedure. Using flash to

demonstrate this procedure is a good way to deepen our understanding.

15
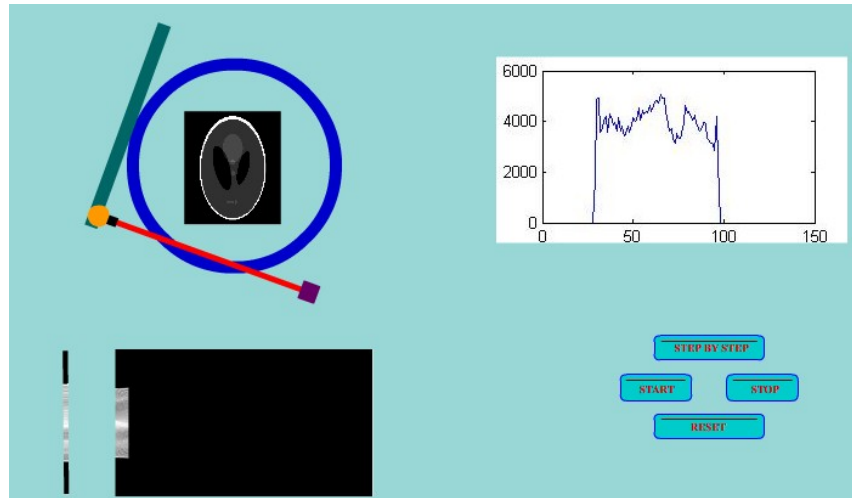
Figure 3.4: Flash simulation of pencil-beam CT projection process. The buttons can control the flash and provide a more comfortable environment for users. The histogram of every slice of the projection is showed after every cycle of scanning.

Pencil-beam CT Scan Reconstruction

In CT imaging, a 3D image of an X-ray absorbing object is reconstructed from a series of 2D cross sectional images[46]. As we deduce above, the content of image's information is changed from system coordinates to polar coordinates. Direct back projection is one of many reconstructed method of CT reconstruction. It is nothing but inverse all the information in radon domain to original system coordinates.

The direct projection equation is like:

$$b_\theta(x,y) = \int_{-\infty}^{+\infty} P_\theta(R,\theta)\delta(x\cos\theta + y\sin\theta - R)dR \qquad (Eq.4)$$

While using direct back projection to do CT reconstruction, we could have two different procedures to do the same reconstructed thing. One option is to extract every projection from radon domain, that is to say, all the information contained in every column in radon domain has the same rotation degree θ, to do direct back projection. Another option is to do the reconstruction by designating specific area in system coordinate. Imaging we have

a known f(x, y) in the detected human section, according to the Equation 3, this particular

point's projection in radon domain should be a line like wave because of the different

rotation degree θ.
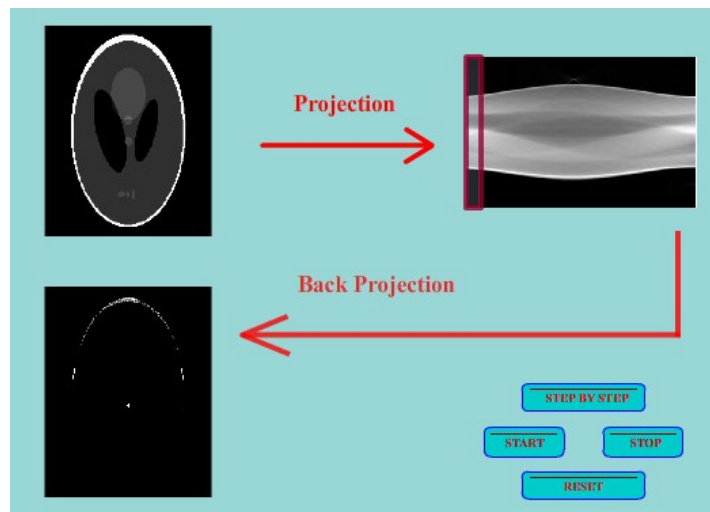
Figure 3.5: Direct back projection of CT reconstruction: extract every projection from radon domain and do the direct back projection..
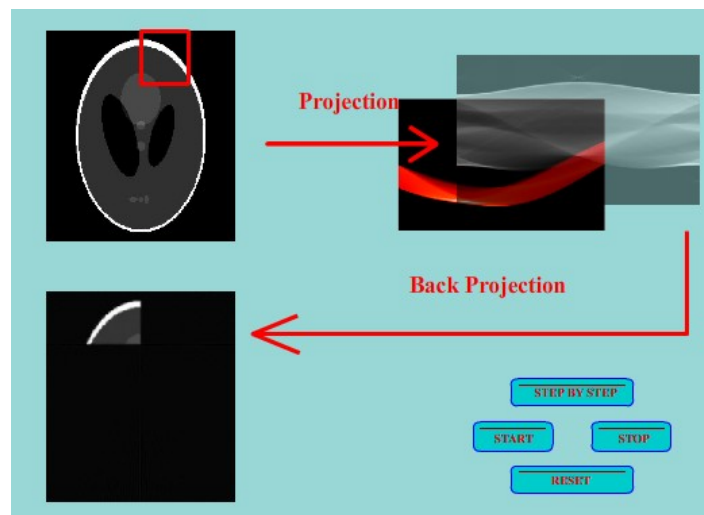
Figure 3.6: Direct back projection of CT reconstruction: extract every "line wave" of each rotation degree to do the direct back projection.

Fan-beam CT Scan Projection

We also create the fan-beam CT projection flash for understanding the operation

principle of the 3rd generation of CT scan. We are not to demonstrate the principle of this

generation of CT scan because we only use the pencil-beam algorithm in our following

experiments for saving programming time and memory space.
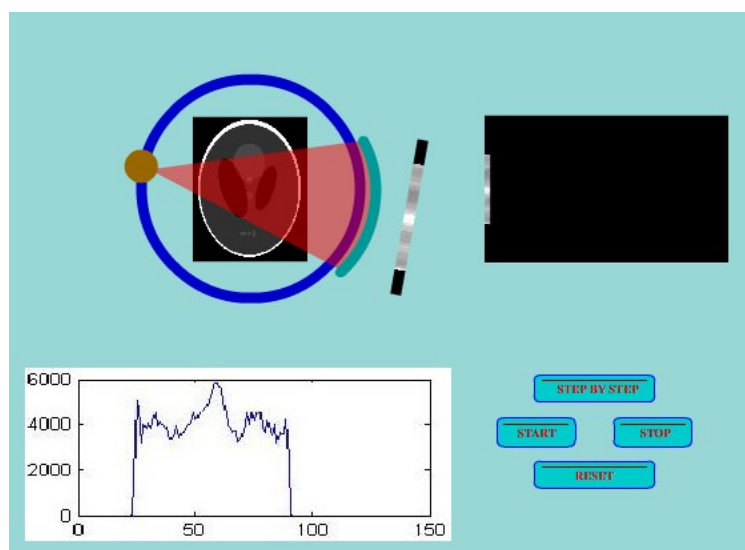
Figure 3.7: Fan-beam CT scan projection: The 3rd generation of CT scan uses a fan-beam X-ray to encompass the entire patient width and using an array of detectors to intercept the fan-beam. The detector array is rigidly linked to the x-ray tube, so that both the tube and the detectors rotate together around the patient.

3.2 System and MI Method Applying to Onsite Image-Registration

As we discussed in Chapter 2, XSI system dominates the radiosurgery field. In order to

register patient's positions between the planning stage and the treatment stage, two

orthogonally projected images from +45° and -45°of the patient under the CyberKnife are

constantly generated during the treatment period. This pair of projection images is then

compared with artificially generated projection images from the CT data during planning

stage, but with various positions.

Van den Elsen et al. (1994) proposed modified correlation techniques using limited ranges of CT intensity representing bone or soft tissue, providing negative or positive correlation respectively with MR. Collignon et al. (1995a) and Studholme et al. (1995) used measures based on the joint entropy of the the combined images. Collignon et al. (1995b) and Viola and Wells (1995) then independently proposed the use of mutual information which relates the joint entropy to the entropy of the two images separately[47].Nowadays, mutual information is a basic concept from information theory, that is applied in the context of image-registration to measure the amount of information that one image contains about the other[48].

3.2.1 Mutual Information Applying in Image Domain: Principle of Entropy, Joint Entropy and Mutual Information

Here we give a brief review of mutual information, which is a measure of the amount of information that one random variable contains about another random variable. It is the reduction in the uncertainty of one random variable due to the knowledge of the other[49]. Mutual information is calculated by entropy, which is a measure of uncertainty of a random variable. The entropy H(X) of a discrete random variable X is defined by:

$$H(X) = -\sum_{x \in X} p(x) \log p(x) \qquad (Eq. 5)$$

Equation 5 defined the entropy of a single random variable. The joint entropy H(X, Y) is defined as:

$$H(X,Y) = -\sum_{x \in X} \sum_{y \in Y} p(x,y) \log p(x,y) \qquad (Eq. 6)$$

Consider two random variables X and Y with a joint probability mass function p(x, y) and marginal probability mass functions p(x) and p(y). The mutual information I(X; Y) is the relative entropy between the joint distribution and the product distribution p(x)p(y):

$$I(X;Y) = \sum_{x \epsilon X} \sum_{y \epsilon Y} p(x,y) \log \frac{p(x,y)}{p(x)p(y)} \qquad (Eq.7)$$

Rewrite the definition of mutual information I(X; Y) as:

$$I(X;Y) = \sum_{x \epsilon X} \sum_{y \epsilon Y} p(x,y) \log \frac{p(x,y)}{p(x)p(y)}$$

$$= \sum_{x,y} p(x,y) \log \frac{p(x|y)}{p(x)}$$

$$= -\sum_{x,y} p(x,y) \log p(x) + \sum_{x,y} p(x,y) \log p(x|y)$$

$$= -\sum_{x,y} p(x,y) \log p(x) + \sum_{x,y} p(x,y) \log p(x|y)$$

We can get:

$$I(X;Y) = H(X) - H(X|Y) \qquad (Eq.8)$$

Thus the mutual information I(X; Y) is the reduction in the uncertainty of X due to the knowledge of Y [49].

By symmetry:

$$I(X:Y) = H(Y) - H(Y|X) \qquad (Eq.9)$$

Finally, we can get;

$$I(X;Y) = H(X) + H(Y) - H(X,Y) \qquad (Eq.10)$$

High mutual information indicates a large reduction in uncertainty; low mutual information indicates a small reduction; and zero mutual information between two random variables means the variables are independent[50].
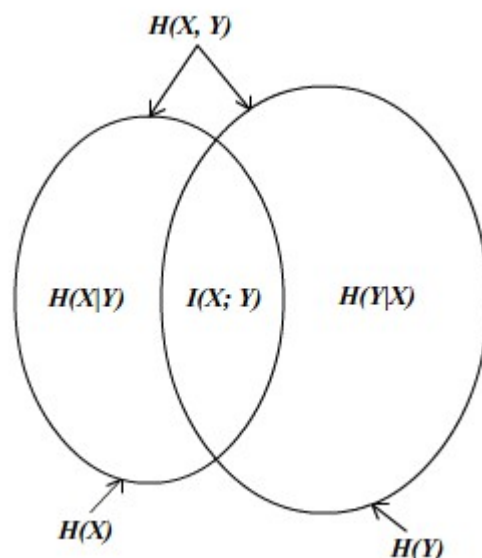
Figure 3.8: Relationship between entropy, joint entropy and mutual information.

3.2.2 The Application of Mutual Information in Image Domain

Mutual information based alignment criteria, a test sample is selected that consists of pixels/ voxels in the overlap of the reference and the floating image. All pixels/voxels in the intersection have the same probability to be included[51]. As we know, gray level images can be identified as the 2D arrays filled with intensity values from the numbers of 0 to 255. I would like to take some examples to explain more clearly about how to perform the calculations of mutual information in image domain.

Assume we have a 3*3 image named "A" with its intensities like this:

0	2	3
1	2	3
1	2	2

Table 1: This table shows the intensity distribution of image A with bit-depth of 2.

We can get this image's histogram, which is the distribution of pixel gray level values for all coordinates:

$$H(g|g = a) = \sum_{all\ pixels} , \quad if\ g = a \qquad (Eq.11)$$

Intensity Value	0	1	2	3
Pixel Numbers	1	2	4	2

Table 2: This table shows the intensity value vs. pixel numbers of image A.

Histogram can be converted to probability density function (pdf):

$$p_R(r) = \frac{H(g)}{total\ number\ of\ pixels} , 0 \leq r \leq 1 \qquad (Eq.12)$$

g ~ r, H(g) ~ p(r)

I	0	1	2	3
P	1/9	2/9	4/9	2/9

Table 3: Intensity value vs. probability density function of image A..

Based on the Entropy equation which has been mentioned above, we have the access to get image A's entropy approximately equals to:

$$E = -\left[\frac{1}{9} * \log_2\left(\frac{1}{9}\right) + 2 * \frac{2}{9} * \log_2\left(\frac{2}{9}\right) + \frac{4}{9} * \log_2\left(\frac{4}{9}\right)\right] \cong 1.8366 \qquad (Eq.13)$$

Now, assume we have another 3*3 image named "B" with its intensities like this:

2	5	7
3	4	1
4	6	6

Table 4: This table shows the intensity distribution of image B with bit-depth of 3.

Similarly, image B's entropy equals to:

$$E = -\left[5 * \frac{1}{9} * \log_2\left(\frac{1}{9}\right) + 2 * \frac{2}{9} * \log_2\left(\frac{2}{9}\right)\right] \cong 2.7255 \qquad (Eq.\,14)$$

So far, we have two images A and B's entropies respectively. Now we are going to "combine" these two images' information, which is to say, to form an "entry" on a 2D histogram and 2D pdf, finally 2D entropy.

The 2D histogram can be calculated by:

$$H_{AB}(g_A|_a, g_B|_b) = \sum_{all\ pixels\ \epsilon\ R\binom{row_A\ \cap\ row_B}{col_A\ \cap\ col_B}} if\ g_A = a\ AND\ g_B = b \qquad (Eq.\,15)$$

3		+						+
2					+	+	++	
1				+	+			
0			+					
	0	1	2	3	4	5	6	7

Table 5: This table shows two dimensional histogram of image A and image B.

If the 2D histogram is divided by the number of pixels within the overlapped area, $H_{A,B}$ becomes a 2D pdf. The projection of the 2D pdf on each axis becomes conditional probability density:

3	2/9		1/9						1/9
2	4/9					1/9	1/9	2/9	
1	2/9				1/9	1/9			
0	1/9			1/9					
		0	1/9	1/9	1/9	2/9	1/9	2/9	1/9
		0	1	2	3	4	5	6	7

Table 6: This is the probability density function of image A and image B.

Joint entropy can be calculated by the equation:

$$H_{A,B} = - \sum_{i=0}^{2^n-1} \sum_{j=0}^{2^n-1} p(a_i, b_j) * \log_2 \left(p(a_i, b_j) \right) \qquad (Eq.\,16)$$

$$Joint - Entropy = - \left(7 * \frac{1}{9} * \log_2 \left(\frac{1}{9} \right) + \frac{2}{9} * \log_2 \left(\frac{2}{9} \right) \right) \cong 2.9477 \qquad (Eq.\,17)$$

As we have, entropy of image A, entropy of image B and joint entropy of image A and B, mutual information between image A and B can be accessed:

$$I(A; B) = E(A) + E(B) - JE(A, B) \qquad (Eq.\,18)$$

$$= 1.8366 + 2.7255$$

$$= 1.6144$$

The mutual information registration criterion presented here states that the mutual information of the image intensity values of corresponding voxel pairs is maximal if the images are geometrically aligned[52].

Chapter 4 Design of Approach for Image-Guided Radiation Therapy

4.1 Partial CT and Radon Transform

4.1.1 Definition of Partial CT

Computerized Tomography (CT) has been widely used in hospitals and clinics. A CT scanner casts a set of X-rays to pass through tissues, bones, and whatever organs. The radiation intensities attenuate to what are measured at the exit by an array of detectors. The measurements form the so-called projection data. Filtered Back-Projection method based on Fourier Slice Theorem is typically adopted to reconstruct the projection data in frequency domain and recover the tomographic information

A modern high-end CT scanner can take several 2D X-ray images around the object by preferably covering 360° (complete rotation). CT systems typically acquire between 360 projections (one projection every degree) and 3600 projections (one projection every 0.1 degree) depending on the final desired resolution.

The degree of CT scanner rotation can decide the final resolution of reconstruction. The more rotation degrees stand for the more 2D X-ray projection acquired, i.e. more information from target saved in bigger radon domain. Abundant amount of information in radon domain and the preferable algorithm involved in the Back-Projection process may reconstruct images with high quality.

24

Partial CT means the rotation degree of CT scanner is less than complete rotation (Pencil-beam's complete rotation is 180°; Fan-beam's complete rotation is 360°). For example, the first generation of CT scanner (Pencil-beam)'s full rotation is 180°, each projection in radon domain corresponds to each degree of X-ray source rotation from 0° to 179°. The Back-Projection is also from 0° to 179° to do the reconstruction correspondingly. When partial CT is from 0° to 89°, i.e. the information from the target saved in radon domain is the half of those with the complete rotation degree from 0° to 179°, the result of this partial CT is a blurry and distorted reconstructed image. With the rotation degree from 0° to 9°, the partial CT reconstructed image can be barely recognized any similarity with the full-rotation reconstructed image.
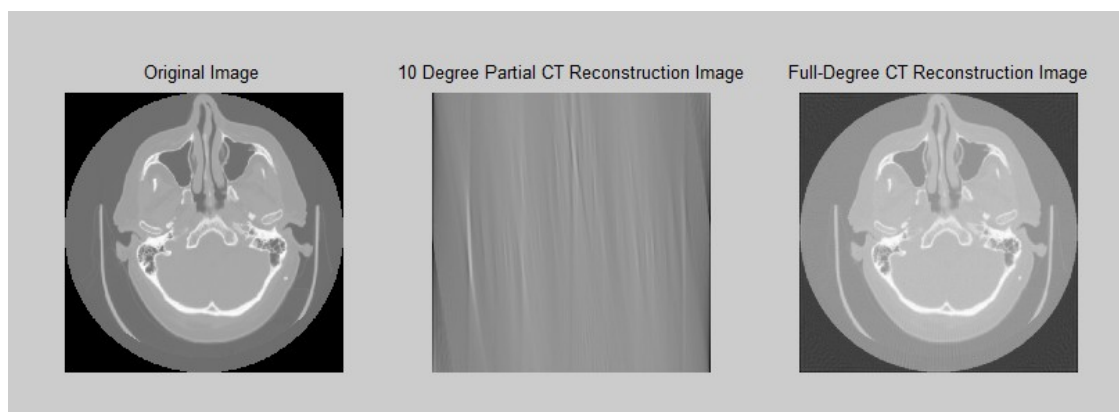
Figure 4.1: From the left to the right: 1) Original image;2) Partial CT reconstructed image with scanning angle of 10°;3) CT reconstructed image with full scanning angle.

In the next designs and following experiment, partial CT with pencil-beam X-ray is assumed to be used for Radiosurgery to obtain the patient's instantaneous positions in order to assure radiation dose delivered accurately at the tumor during the surgery.

4.1.2 Radon Transformation Definition

The Radon transform is an integral transform whose inverse is used to reconstruct images from medical CT scans[53]. The Radon transform is named after Johann Radon (1887–1956), an Austrian mathematician who wrote a classic paper in 1917 on the inverse problem of determining a two dimensional function from the knowledge of its line integrals. The inverse problem of Radon transform arises in widely diverse fields which include medical imaging, astronomy, crystallography, electron microscopy, geophysics, optics, and material science where the general problem of unfolding the internal structure of an object by its projections is known as the problem of reconstruction from projections[54]. The Radon transform data is often called a sinogram.
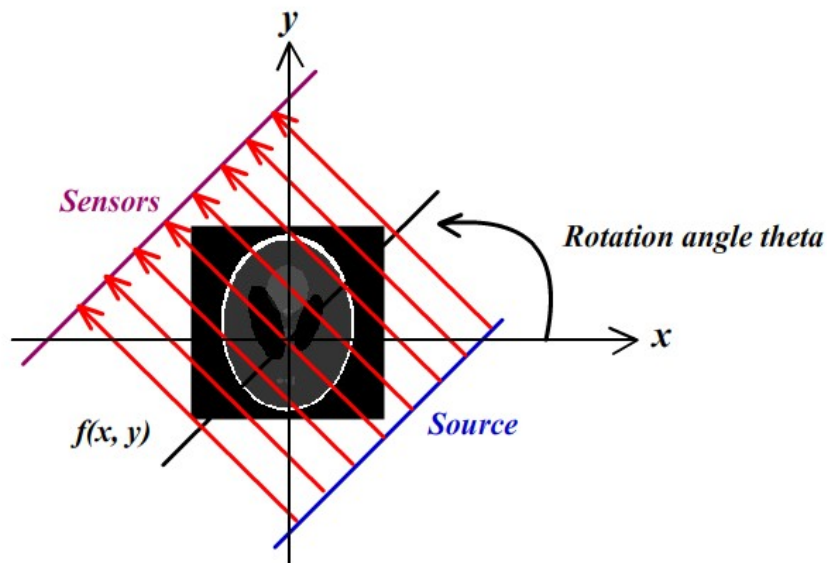
Figure 4.2: Pencil-beam projection at rotation angle theta. In MATLAB the radon function computes the line integrals from multiple sources along parallel paths

In MATLAB platform, the radon function computes projections of an image matrix along specified directions. A projection of a two-dimensional function f(x, y) is a set of line integrals. The radon function computes the line integrals from multiple sources along parallel paths, or beams, in a certain direction. The beams are spaced 1 pixel unit apart. To represent an image, the radon function takes multiple, parallel-beam projections of the image from different angles by rotating the source around the center of the image. The following figure shows a single projection at a specified rotation angle[55].

Thus, our partial CT's projections can be acquired by computing the Radon transform of an original CT scan image for the angles specified in the vector theta using the radon function with this syntax.

MATLAB code: R = radon (I, theta1:theta2);

Identically, our partial CT's back projections also have been generated by using the radon function in the same angles of theta.

MATLAB code: IR = iradon(R, theta1:theta2);

In the experiments in Chapter 5, the "radon" and "iradon" function of MATLAB allow us to prepare the data set in planning stage by creating the narrow-angle partial CT sinogram matrixes and reconstruction matrixes from the original CT data.

4.2 Onsite Image-Registration Designs

This section presents some designs for acquiring partial CT data based on one set of X-ray source and radiation detectors. Contrasting to conventional CT's set up, where an X-ray source rotates around the subject, our partial CT device sets the X-ray source stand

still or rotates slightly and uses a robot-assisted couch to collect projection data at the same time.

Following sections show the designs (with rotating X-ray source or with rotating couch). The designs are made as close to realistic dimension as possible.

4.2.1 Cambered Detector Attaches to the Back Side of the Robotic Couch

The detector is adhered to the reverse side of the robotic couch. As the figures illustrate below, a circle model with 0.48 meter radius was established to explain the geometrical relationship of this design.

The detector is bended as an arc corresponding to the 140° central angle in this particular circle model. X-ray tube applies to rotate from 5° to -5° along the top of this circle, around the center, performing as a partial fan-beam CT scan. The filed angle of X-ray is 60° from the tube which could guarantee to cover the whole pertinent part of patient during the scanning period.

About the area of detector board:

Plan A: Cambered detector board attaches to the back side of the robotic couch without independent movement. If the couch is 2 meters long, and the radiosurgery usually involves brain to chest treatments, the length of the detector board should be at least 1meter to match the size of the upper part of the patient's body. The width of the board is the same as the couch.

Plan B: As we mentioned above, the detector board is acting as a part of partial CT scan to match up the X-ray emitting from the tube, which means 5cm to 10 cm of the length of the board is long enough to detect the X-ray source. In that case, the detector board

should be designed to be capable of moving frontward or backward along the couch to a position suiting the right scanning part during the treatment. The width of the board is the same as the couch.
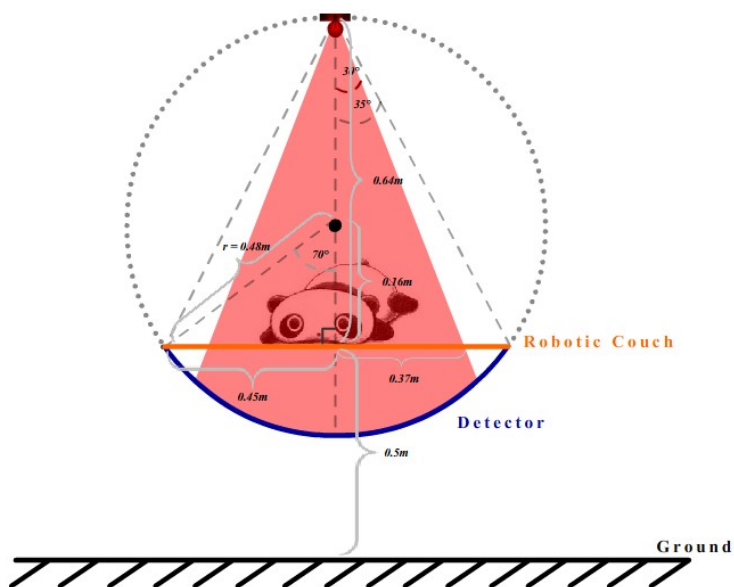
Figure 4.3: Cambered detector attaches to the back side of the robotic couch; X-ray tube stays right above the couch before the radiosurgery treatment.

In this design, X-ray tube is the only rotated part in the system around the circle.
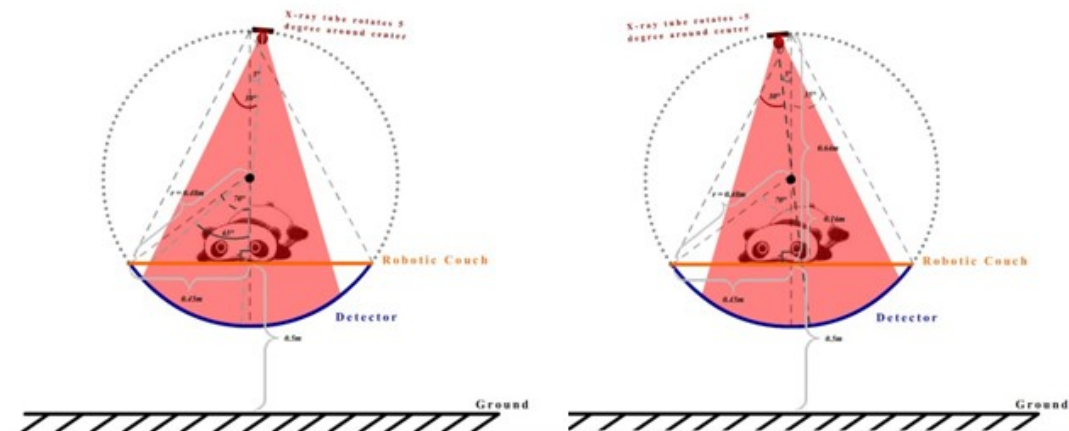
Figure 4.4: From the left to the right: 1) X-ray tube rotates to the location of 5°; 2) X-ray tube rotates from 5° to 5° by 1° increment to fulfill the partial CT scan. The partial CT scanning angle is 11°.

4.2.2 Flat Detector Parallels to the Robotic Couch

The detector board is hanging 6cm beneath the couch and can do the rotation around the center of the board. According to the geometric relationship in the figure, the width of the board could be shorter than the width of the couch.

To simulate the partial CT scanning, detector board rotates simultaneously with the X-ray tube around the center of the circle from 5° to -5°. This relative motion uses the same principle as the 3rd generation CT scanner.

About the area of detector board:

Plan A: The detector board is half size of the couch.

Plan B: The length of the board is around 10cm. The detector board should move frontward or backward along the couch to a position for suiting the right scanning part during the treatment.
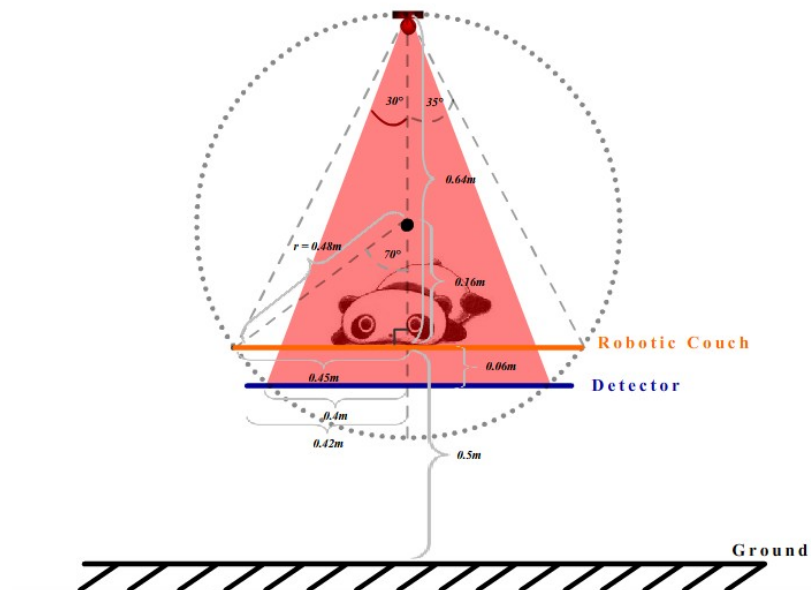
Figure 4.5: Flat detector parallels to the robotic couch; X-ray tube stays right above the couch before the radiosurgery treatment.

X-ray tube and detector board rotates at the same time and same degree around the center of circle during radiosurgery treatment.
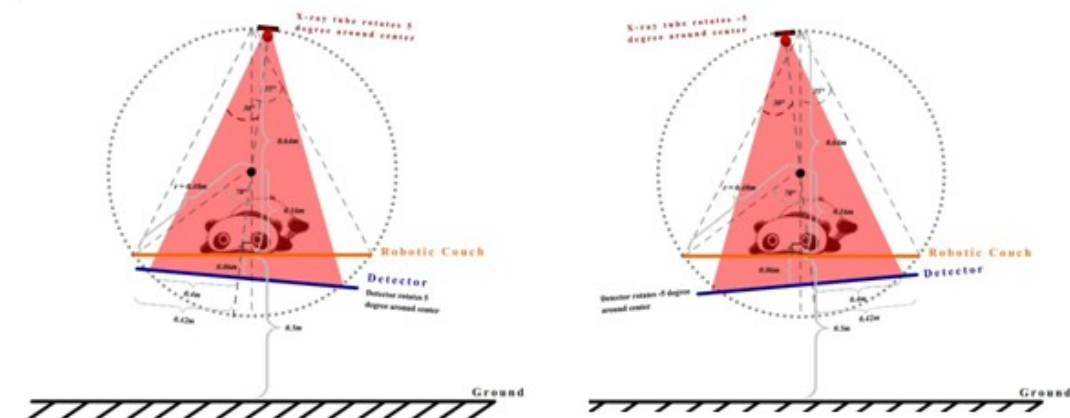
Figure 4.6: From the left to the right: 1)X-ray tube rotates along with detector board to the location of 5°; 2) X-ray tube rotates along with detector board from 5° to -5° by 1°increment to fulfill the partial CT scan. X-ray tube and detector board rotates synchronously. The partial CT scanning angle is 11°.

4.2.3 Flat Detector Fixes on the Ground

The detector board in this design is shaped as a flat board with at least 1.4 meter width fixed stably on the ground.

During the image-registration process, the robotic couch rotates only in this system. It rotates from 5° to -5° around the center of the circle, as the figures illustrate below, is the same relative movement with the 3rd generation of CT scanner. The figures below explain the geometrical relationship of the design system. Rotating robotic couch is same with rotating the X-ray tube to simulate partial CT procedure.
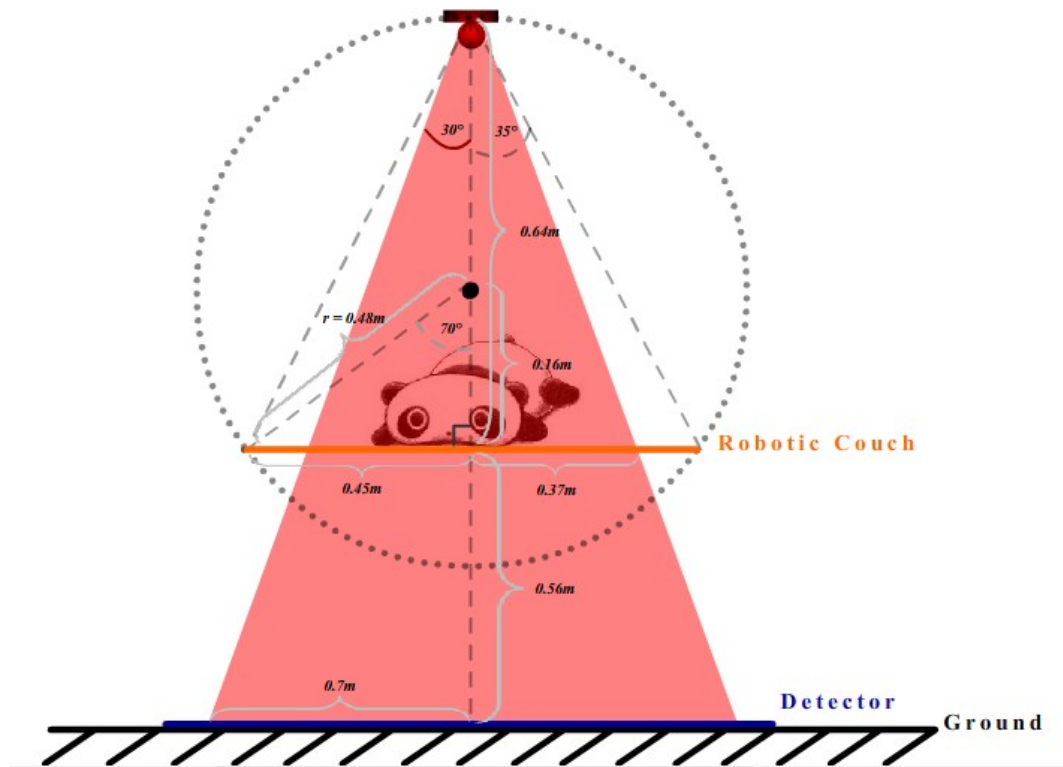
Figure 4.7: Flat detector fixed on the ground. X-ray tube keeps static during the radiosurgery. Robotic couch rotates solely in this design's system. Detector board stays parallel with ground before the radiosurgery.

Robotic couch rotates around the center of the circle, only
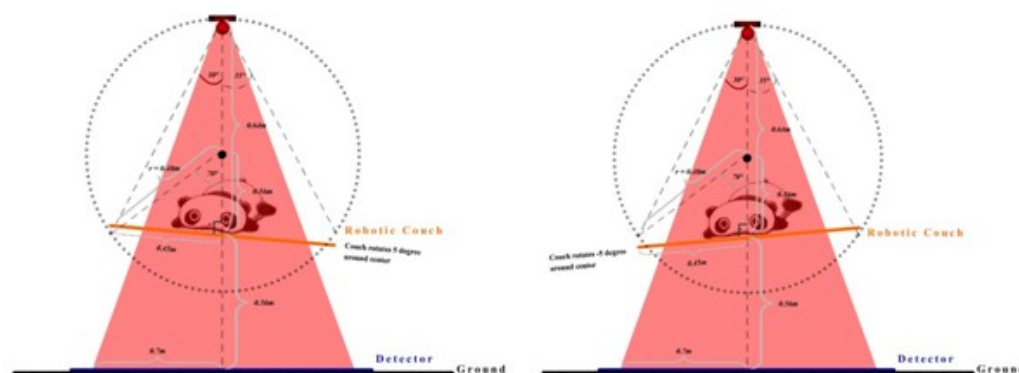
Figure 4.8: From the left to the right: 1) Detector board rotates 5° towards the right; 2)Detector board rotates from 5° to the -5° by 1° increment to fulfill the partial CT scan. The partial CT scanning angle is 11°.

4.2.4 Cambered Detector Attaches to the Ground

In this design, detector board is on the ground and shape as an arc regards to the circle of

0.6 meter radius. As the geometrical relations illustrate in the figures below, the field

angle of X-ray source is 50 degree, the robotic couch's width is 0.7 meter, and the base of

the detector is 1 meter width, 0.26 meter maximum height. Robotic couch and detector

base are stationary during the image-registration processing.

To simulate the partial CT scanning, X-ray tube rotates from 5 degree to -5 degree around

the center of this circle. This is just like the principle of 4th generation CT scanner, by

partial.
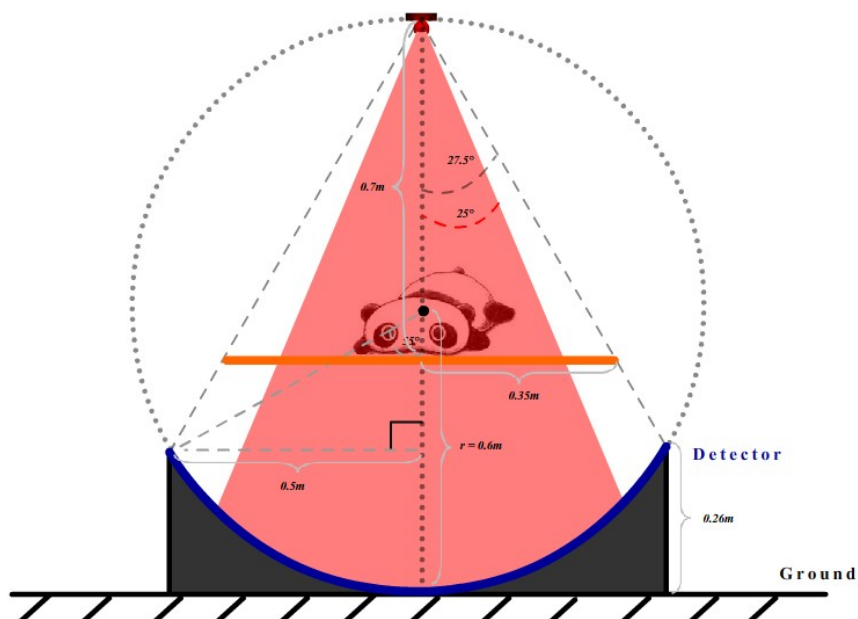
Figure 4.9: Cambered detector attaches to the ground. X-ray tube rotates only in this design's system. Robotic couch stays without movement during radiosurgery treatment.

X-ray tube rotates from 5 degree to -5 degree around the center of the circle, only.
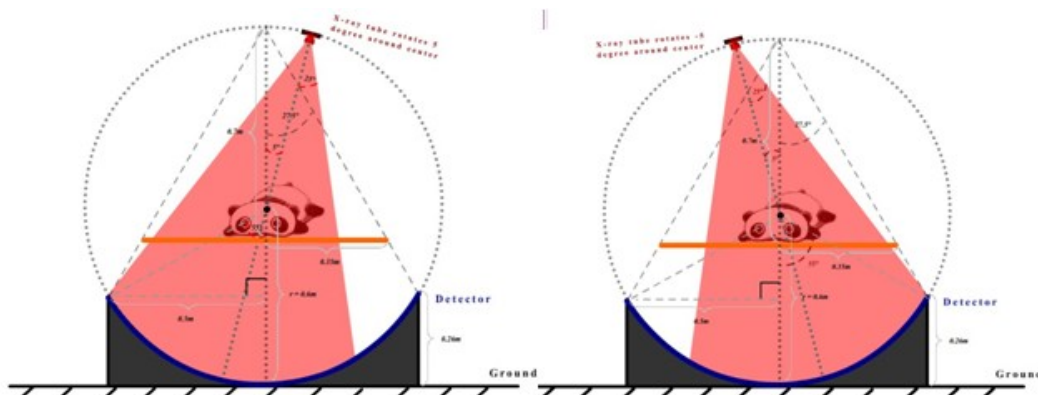
Figure 4.10: From the left to the right: 1) X-ray tube rotates to the location of 5° rightwards; 2) X-ray tube rotates from 5° to -5° by 1° increment to fulfill the partial CT scan. Cambered detector board and robotic couch keeps static during the treatment. The scamming angle of partial CT is 11°.

Chapter 5 Simulation Results

5.1 Simulated Experiment between XRI System and MI Method by MATLAB

Application Programming Interfaces: MATLAB.

To provide a convenient way of programming the graphics and generating DRR images, an application programming interface (MATLAB) is needed. MATLAB (matrix laboratory) is a high-level language and interactive environment for numerical computation, visualization, and programming[56].
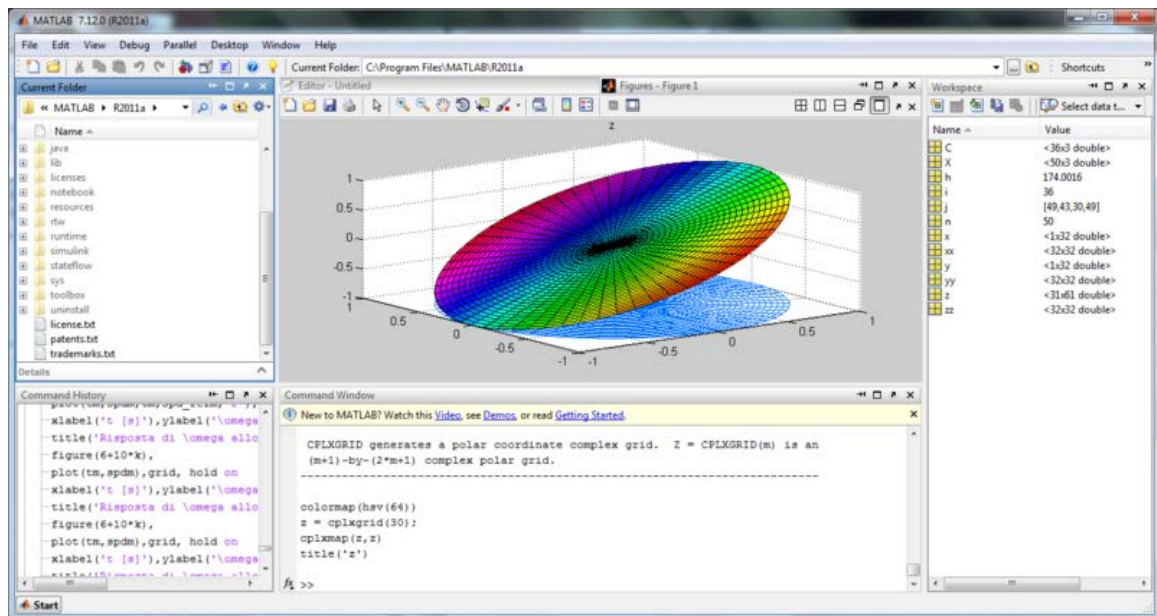
Figure 5.1: MATLAB interface. You can use MATLAB for a range of applications, including signal processing and communications, image and video processing, control systems, test and measurement, computational finance, and computational biology.

5.1.1 The Provenance of the Original Data Matrix

The source of 44-slice of real human's brain phantom was downloaded from the National Cancer Institute (NCI)'s open-sources database. We loaded all 44 slices CT scan images as a data matrix to the MATLAB environment. The matrix contains following information: the format of data type is int16; the matrix's dimension is 512*512*44, FOV is 250mm tall by 250mm long by 155mm wide; the maximum intensity value is 4095, the minimum intensity value is -2000.This set of data are named as the original data matrix.

5.1.2 The Artificial Data Set Matrix

One problem of getting the projection images from the original data matrix is that the resolutions from three different dimensions are not uniform. In order to unify the resolution, we artificially interpolate the dataset. The method of interpolation is to process every single slice of the original matrix into 7 images by averaging two pixels with the same coordinates in the two adjacent slices. Finally, a new resolution-uniformed matrix has been built up with dimension of 512*512*308, e.g., the resolution of this new matrix is 0.5mm/pixel in all three dimensions.

This matrix contains 308 slices of interpolated CT images. We named this one as interpolated data matrix.
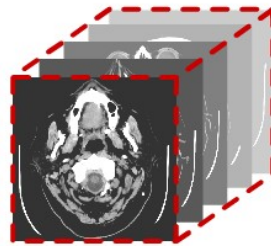
Figure 5.2: Interpolated data matrix. The dimension of this matrix is 512*512*308, and the resolution is 0.5mm/pixel in all three dimensions.

5.1.3 The Planning Stage

The first thing to set up the planning stage is to simulate the gold seeds and the rotation cases during the treatment. To achieve these, we decide to embed "fiducial markers" in the interpolated data matrix and the patient's rotation degree should be changed from - 10° to +10° with 1° increment at each time, which means 21 rotated matrixes with the dimensions of 512*512*308 have been generated and saved. I would like to emphasize that the rotation is the only variable in this experiment.

In radiation therapy treatment, several gold seeds are embedded into the patient as fiducial markers. Thus, we simulate this by inserting 3 small cubes (voxel size of $3\times3\times3$), as high density metal markers, in different locations. The first cube is inserted between No.99 slice and No.101slice, at the top left corner of the matrix; the second cube is inserted between No.149 slice and No. 151 slice, in the middle of the matrix; the last one is inserted between No.199 slice and No. 201 slice, at the bottom right corner of the matrix. Each of the voxel is assigned image intensity of 13 times higher than the maximum intensity level in the whole image data set, to simulate the scenario that the gold seeds' density is approximate 13times bigger than human bone's density.
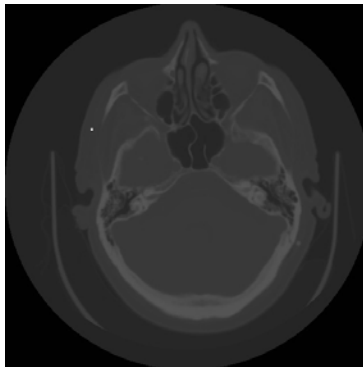
Figure 5.3: Interpolated CT image with fiducial marker. This is the No. 99 slice in interpolated data matrix. The size of fiducial marker in this image is 3*3 pixels.

In the second step, we rotate the above matrix that includes "golden seeds" from -10° to +10°. 21 matrixes have been generated and saved, and the interpolated matrix with no rotation has been included too. These matrixes are ready to be projected by two orthogonal X-ray stereotactic imagers in the next step.
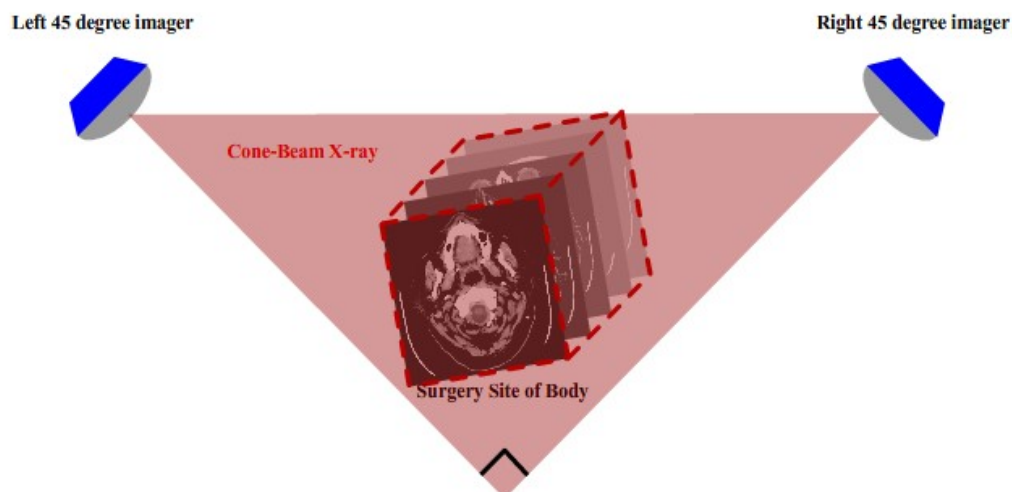
Figure 5.4: Interpolated data matrix is rotated to -10°. Two orthogonal X-ray stereotactic imagers cast a pair of projections at -45° from the left side and at 45° from the right side.

The process in step 3 is to generate two projection images at -45° and +45° respectively of each rotated matrix. Every two projection images at the particular patient's rotation degree are called paired images. Thus, 21pairs of projections should be generated at the end of this planning stage. As the images show, three light spots can be recognized easily in the projection images.

The algorithm used here is a simple case of ray casting. The pseudocode of this algorithm can be found in appendix.
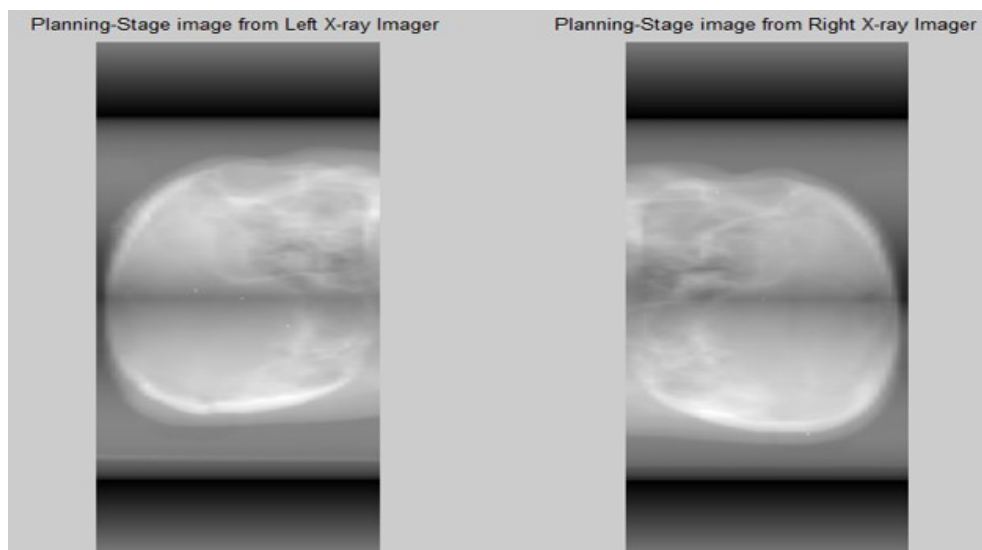
Figure 5.5: DRR image are obtained by these two orthogonal X-ray stereotactic imagers. Three light spots can be recognized easily in the projection images.

Using LUT or excel table to designate the particular rotation degree of each pair of projection is the final step to complete the planning stage. The advantage of this "taking one's seat according to the number on the ticket" helps users to acquire the patient's rotation directly and promptly as long as the number of the pair has been picked up.

5.1.4 The Treatment Stage

In order to register patient's positions between the planning stage and the treatment stage, two orthogonally projected images from +45° and -45°of the patient under the CyberKnife are constantly generated during the treatment period.

In this experiment, we randomly select one pair of projection set up already in planning stage as the instantaneous projection pair obtaining during radiosurgery treatment.

The pair of projection obtained at treatment stage is randomly chosen by our MATLAB program from the 21 pairs of projection set up in the planning stage. We may not know

which pair has been chosen by computer right now, however in the end of this experiment, after achieving the experiment's result, then we can get the access to know this randomly computerized-selected pair of projection by scanning the coding record and use this record as the authentic answer to evaluate the validity of our experiment's result.

A) Current Algorithm of XSI

In image guidance system, after attaining the projections pair in the treatment stage, making comparison of two stages' projections pair to find the patient's instantaneous movement is the ultimate goal.

These two projection images serve as the 3D positioning basis of the patient in the planning stage. In the next, we are going to use this pair of projection to compare with the pair of projection with no patient's movement and calculate the patient's rotation angle by using XSI algorithm.

The figure and equations below describe the rational relationship between the high intensity pixels (projection of small cubes) in planning stage and treatment stage, by which patient's rotational position can be corrected during radiosurgery procedure.

The angle θ means the rotation angle of the fiducial marker. Thus, when theta equals to -45° and 45°, we can get point A's x-axis in the two projection images without patient's movement. These two x-axes of A point are known in the planning stage.

Planning stage:

Imager at left -45°: $X_L = X * \cos(45°) + Y \sin(45°) = \frac{\sqrt{2}}{2}X + \frac{\sqrt{2}}{2}Y$

Imager at right 45°: $X_R = X * \cos(-45°) + Y \sin(45°) = \frac{\sqrt{2}}{2}X - \frac{\sqrt{2}}{2}Y$
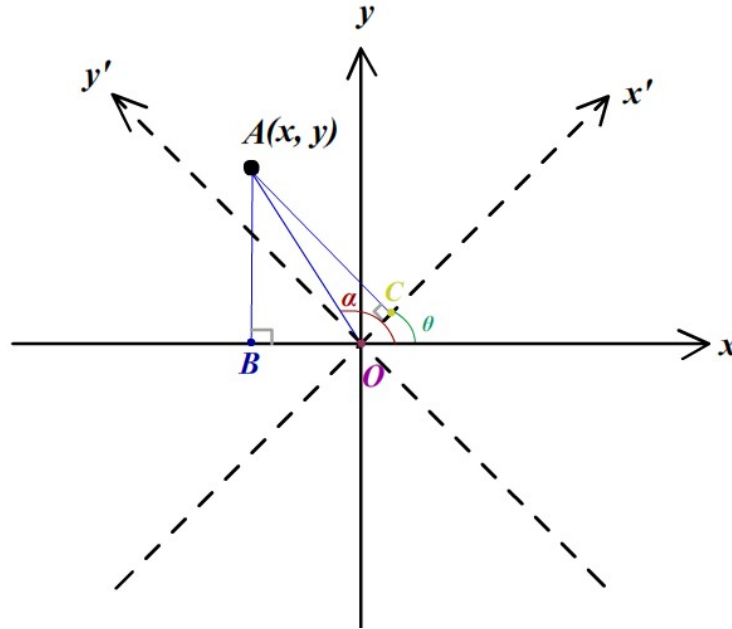
Figure 5.6: Point A in the original coordinate and the rotated coordinate.

Assuming there is an angle φ, which is the patient's rotation angle during the radiosurgery treatment. We can deduce the relationship between A's x-axes in treatment stage and the rotation angle φ.

Treatment stage:

Imager at left -45°:

$$X'_L = X * \cos(45° + \varphi) + Y \sin(45° + \varphi)$$

$$= [X * \cos(45°) + Y \sin(45°)] \cos(\varphi) + [-X \sin(45°) + Y \cos(45°)] \sin(\varphi)$$

$$= \left(\frac{\sqrt{2}}{2} X + \frac{\sqrt{2}}{2} Y\right) \cos \varphi + \left(-\frac{\sqrt{2}}{2} X + \frac{\sqrt{2}}{2} Y\right) \sin \varphi$$

$$= X_L * \cos \varphi - X_R * \sin \varphi$$

Imager at right 45:

$$X'_R = X * \cos(-45° + \varphi) + Y \sin(-45° + \varphi)$$

$$= [X * \cos(-45°) + Y \sin(-45°)] \cos(\varphi) + [-X \sin(-45°) + Y \cos(-45°)] \sin(\varphi)$$

$$= \left(\frac{\sqrt{2}}{2}X - \frac{\sqrt{2}}{2}Y\right) \cos \varphi + \left(\frac{\sqrt{2}}{2}X + \frac{\sqrt{2}}{2}Y\right) \sin \varphi$$

$$= X_R * \cos(\varphi) + X_L * \sin(\varphi)$$

Therefore, we can get φ's values:

$$\varphi_{1.2} = \arcsin\left(\frac{X_L * X'_R - X_R * X'_L}{X_L^2 + X_R^2}\right) \qquad (Eq. 19)$$

$$\varphi_{3,4} = \arccos\left(\frac{X_L * X'_L + X_R * X'_R}{X_L^2 + X_R^2}\right) \qquad (Eq. 20)$$

In the Eq.19 and Eq.20, φ are four degrees should have been acquired because two

different degrees have the same value in [-π, π] interval of sine and cosine function. X

and X' are the coordinates of high intensity pixels in two corresponding stages'

projections.

As simulated in the experiment, the interval of φ in this study is [-10°, 10°]. Thus the φ's

value can be acquired by getting rid of the other φ's value who's not in the internal of [-

10°, 10°]. The very small increment value of cosine curve, and in contrast, the very

distinct increment value of sine curve in the interval from -10° to 10° can explain the

reason why the φ's value from Eq.1 is much more accurate than the value from Eq.2.

The result of using XSI algorithm is φ = 7°. Let's move on to the next MI experiment and

use this result to test and verify the accuracy of MI method.

B) Mapping Maximum MI in Image-Registration Field

In the treatment stage, we randomly choose one pair of X-ray images from the planning stage, as the target image pair. We then calculated the MI with every image pairs, i.e., all 21 image pairs in the planning stage. The MI calculation was based on the following equations:

$$I_L(X_L; Y_L) = H(X_L) + H(Y_L) - H(X_L, Y_L) \qquad (Eq.\,21)$$

$$I_R(X_R; Y_R) = H(X_R) + H(Y_R) - H(X_R, Y_R) \qquad (Eq.\,22)$$

$$I = I_L + I_R \qquad\qquad\qquad\qquad (Eq.\,23)$$

Where H is entropy of an individual image, or joint entropy of two images; I is mutual information between two images.
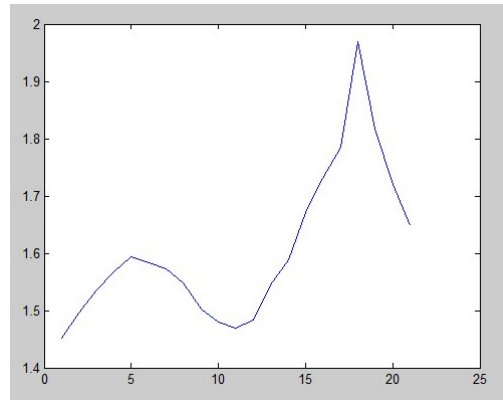
Figure 5.7: MI map of target pair and 21 image pairs in the planning stage. The maximum mutual information shows as the peak at the 18th pair, which means the target pair and the 18th pair in planning stage has the most similarity.

The maximum mutual information in this graph indicates that the eighteenth pair of projection images in the planning stage has the most similarity to the image pair randomly selected. As we export the Look Up Table we wrote in the planning stage, it is clearly to know that the patient's rotation degree is 7° corresponding with No. 18th pair of projection. The value of 7° is the same as the value we had got by utilizing the current

algorithm. Also, the coding record indicates that the random rotation angle selected by MATLAB is 7 ° too. This experimental result indicates that patient's onsite 3D position can be determined by the maximum MI matching procedure.

5.1.5 Conclusion

We can use a flow chart to make the process of this experiment more clearly.
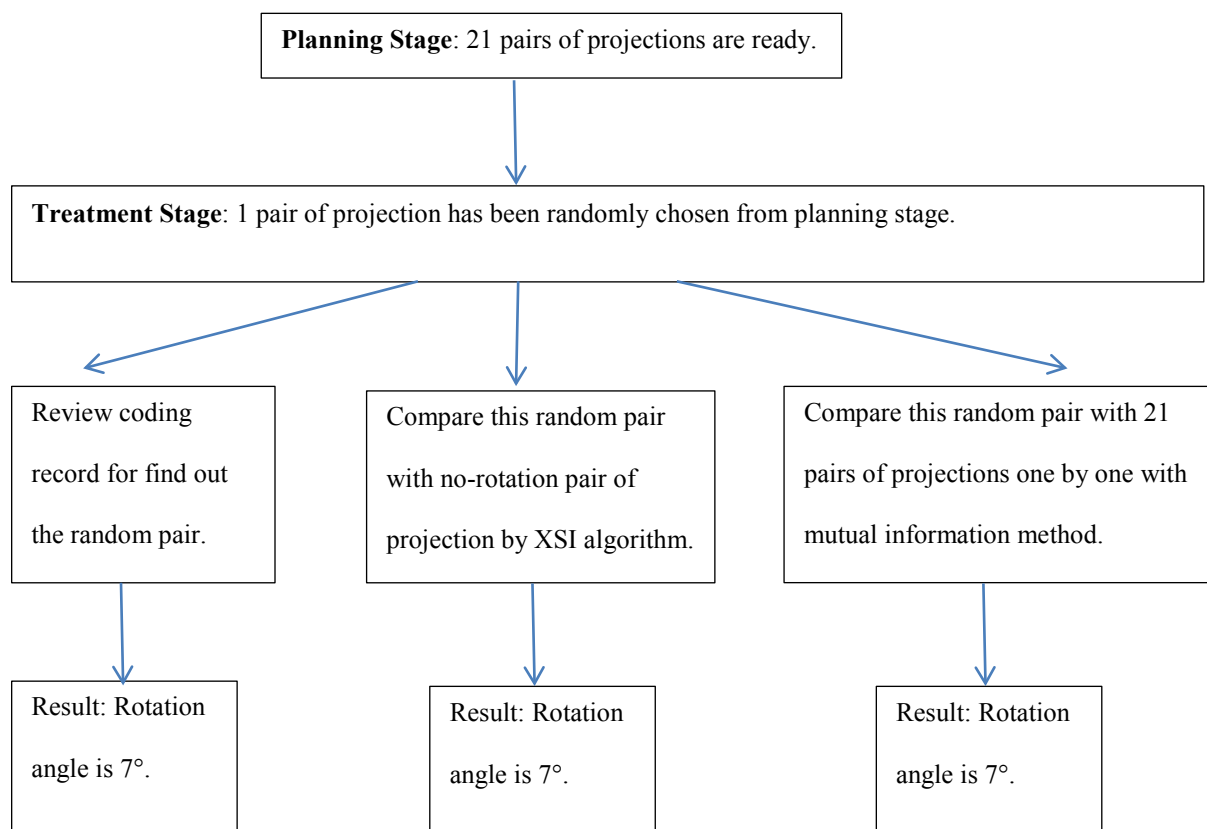
Figure 5.8: The process of the first experiment is showed by flowchart. It includes the planning stage and treatment stage and the result of this experiment.

The mutual information is a reliable indicator for image matching. This method can be utilized in image guide system of radiosurgery by comparing orthogonally projected image pairs to obtain onsite 3D position information so as to assure radiosurgery's accuracy.

5.2 Mapping Maximum Mutual Information between Partial CT Images

In the first section of this Chapter, we have discussed that the limited-scanning-angle partial CT reconstruction images are hard to be recognized. However, we asked previously that if the partial CT reconstruction images acquired at the patient's treatment stage, the images can match the partial CT data generated from the full-scanning CT images. We use the feasible method demonstrated in the previous section, mutual information, to find the most similar images by mapping all the intensities in the images. We are going to perform this MI method in this following experiment to verify that the narrow-scanning-angle partial CT's reconstruction images and even the sinogram image may still possess enough information to be utilized by mapping maximum mutual information.

5.2.1 Planning Stage

The planning stage includes three matrixes which are original CT data matrix, partial CT projection matrix and partial CT reconstruction matrix with scanning angle from -10° to 10°. To get this straight, let's name the original CT data matrix is the "A" matrix; name partial CT sinogram matrix as "B" matrix; partial CT reconstruction matrix is the "C" matrix. Every matrix consists of 44 images.

These three matrixes' data format has been uniformly converted to uint8 format in order to perform mutual information computation. The pseudocode of this altering process can be found in appendix.

5.2.2 Treatment Stage

One original CT image has been selected randomly from "A" matrix as the patient's instantaneous X-ray image during the radiation treatment, called "a" image. Partial CT sinogram ("b" image) and reconstruction ("c" image) are attained at the same time by MATLAB code at the rotation angle from -10° to 10°. This is to say, we now have three patterns of patient's instantaneous images waiting for comparing with the three matrixes built in planning stage. Also, these three images have been converted into uint8 format. Finding the most similar images between image from planning stage's matrix and treatment stage image by calculating the entropy, joint entropy and mapping the maximum mutual information has been conducted. In other words, "a" image is mapping the mutual information with every images in "A" matrix; "b" image is mapping the mutual information with every images in "B" matrix; in a similar way, "c" image is mapping the mutual information with every images in "C" matrix. After three mapping, we plot all the values of mutual information between these images, and the maximum value of mutual information occurs in the same location in these three curves.
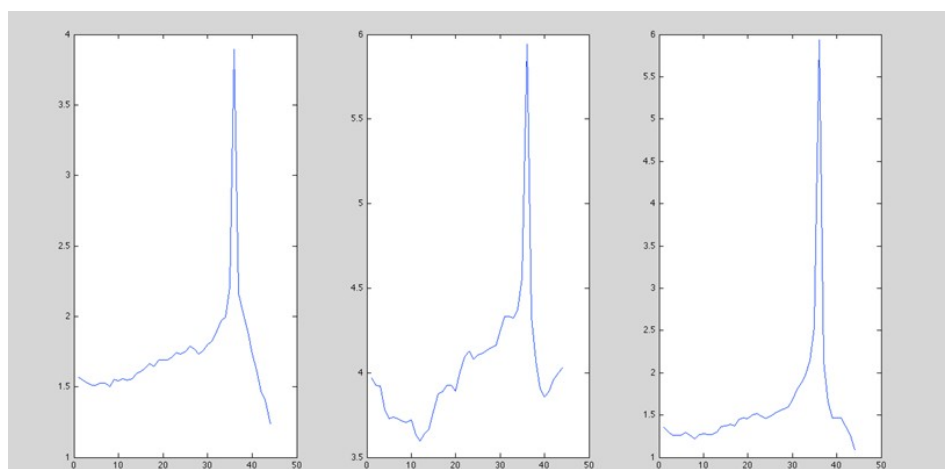
Figure 5.9: From the left to the right: 1) The curve of MI values between "a" and "A"; 2) The curve of MI values between "b" and "B; 2) The curve of MI values between "c" and "C". The maximum mutual information occurs at the location of No.36 in all three maps.

5.2.3 Results and Conclusion

Let us review this experiment's process by following the flow chart and analyze the result of this experiment.

Figure 5.10: The flow chart of the second experiment's process.

```
                    ┌─────────────────────────────────────────┐
                    │ Planning Stage: Three matrixes are ready. │
                    └─────────────────────────────────────────┘

  ┌──────────────────┐   ┌──────────────────┐   ┌──────────────────┐
  │ Matrix "A":       │   │ Matrix "B": matrix│   │ Matrix "C":  matrix│
  │ Original CT data  │   │ A's Partial CT    │   │ A's Partial CT    │
  │ matrix.           │   │ sinogram matrix   │   │ reconstructed     │
  │                   │   │ with scanning     │   │ matrix with       │
  │                   │   │                   │   │ scanning angle    │
  └──────────────────┘   └──────────────────┘   └──────────────────┘

                    ┌──────────────────────────────┐
                    │ Treatment Stage: three images. │
                    └──────────────────────────────┘

  ┌──────────────────┐   ┌──────────────────┐   ┌──────────────────┐
  │ Image "a": an     │   │ Image "b": image  │   │ Image "c": image  │
  │ image randomly    │   │ a's partial CT    │   │ a's partial CT    │
  │ selected from     │   │ sinogram with     │   │ reconstructed     │
  │ matrix "A".       │   │ scanning angle of │   │ image with        │
  │                   │   │ 21°.              │   │ scanning angle of │
  │                   │   │                   │   │ 21°.              │
  └──────────────────┘   └──────────────────┘   └──────────────────┘

  ┌──────────────────┐  ┌──────────┐  ┌──────────┐  ┌──────────┐
  │ Review coding     │  │ "a"       │  │ "b"       │  │ "c"       │
  │ record to find out│  │ compares  │  │ compares  │  │ compares  │
  │ the random        │  │ with "A". │  │ with "B". │  │ with "C". │
  │ image.            │  └──────────┘  └──────────┘  └──────────┘
  └──────────────────┘

  ┌──────────────────┐  ┌──────────────┐  ┌──────────────┐  ┌──────────────┐
  │ Result: The       │  │ Result: No. 36│  │ Result: No. 36│  │ Result: No. 36│
  │ random image is   │  │ is the        │  │ is the        │  │ is the        │
  │ No.36 slice in    │  │ location the  │  │ location the  │  │ location the  │
  │ matrix "A".       │  │ maximum MI    │  │ maximum MI    │  │ maximum MI    │
  │                   │  │ occurred.     │  │ occurred.     │  │ occurred.     │
  └──────────────────┘  └──────────────┘  └──────────────┘  └──────────────┘
```

From the MI maps, number 36 is the location of the maximum value of mutual information from three mutual information curves. According to the MATLAB coding record, the randomly chosen image of the original CT scan matrix is numbered 36, too. This particular image and its sinogram and reconstruction pattern have been found exactly and accurately from the matrixes in planning stage by mapping the maximum mutual information.

This experiment has demonstrated that the narrow-angle partial CT sinogram and reconstruction images still hold sufficient information that can utilized by mutual information method in the image registration field although these partial CT images can be barely recognized.

5.3 Simplified Onsite Image-Registration Approach for Radiosurgery

In this section, we are going to prepare more complicated planning stage matrixes to simulate the possibilities of patient's rotation and translation. For the three images acquired from treatment stage, can we prove that mutual information is still working between these partial CT sinograms and reconstructions with very small variations?

In order to illustrate the process as much as possible, the design in the Chapter 4 has been chosen and highlighted as the basic design and the foundation of our theory. That is, during the radiation treatment, the patient is lying on the robotic couch which could rotate a narrow angle to simulate the same affection as the relative movement of partial CT scan. Only one X-ray imager is needed and the X-ray beam is considered as Pen-beam.

The detector board underneath the robotic couch receives the partial CT's instantaneous projections along with the every rotation degree of the couch.
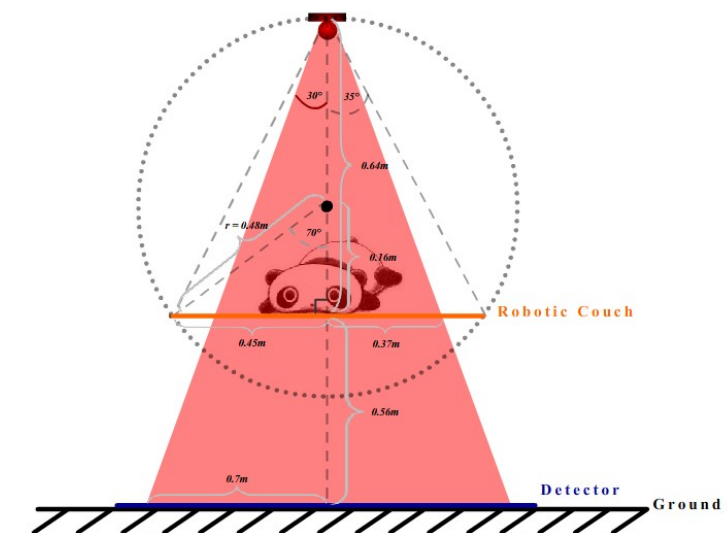
Figure 5.11: The design to simplify the onsite image registration approach for radiosurgery. The couch may rotate a narrow angle during the treatment, only one X-ray imager is needed to perform the partial CT scan.

5.3.1 Planning Stage

In the first section of this Chapter, we have introduced a matrix consists of 44 images of brain CT scan with int16 format and called original CT data matrix. Now we use every slice of this original matrix to do some rotations and translations to simulate the patient's movement in reality. Shifting columns circularly by variable quantity of [-10 -5 0 5 10] is supposed to mimic the X direction movement; in a similar way, shifting rows circularly by variable quantity of [-10 -5 0 5 10] is supposed to mimic the Y direction movement; rotating images by variable quantity from -5° to 5° with 1° increment might be considered as the simulation of patient's rotation. To fulfill these simulations, we wrote a program to run all combinations of these variables. As we illustrate, there are 275 combinations by every image from the original CT scan matrix. Thus, the first step to

build this experiment's planning stage is to create 44 matrixes with 512*512*275 voxels (0.5mm/pixel*0.5mm/pixel*-3.5mm/pixel resolution). We prefer to call these matrixes as "1st step matrixes". All of 44 matrixes have been saved as .mat file in MATLAB.

The second step is to generate partial CT sinogram matrixes. When we are processing these sinogram matrixes, one question arises regarding the range of effective scanning angle. The narrower of the scanning angle, the less information contains in the partial CT sinograms. What is the threshold of the scanning angle of partial CT that may satisfy the mutual information method in this image registration experiment? We designate the scanning angle that the biggest angle is 21°and the smallest angle is 3°in sequence, e.g., the first scanning angle is from -10° to 10°, the second scanning angle is from -9° to 9°, one by one. Therefore, in this step, every matrix from "1st step matrixes" has ten "sinogram matrixes" with different scanning angle.

The "reconstruction matrixes" are set up corresponding with "sinogram matrixes" in the last step.

All those images from the matrixes in planning stage should be converted to uint8 format and saved as .mat files as stand-by.

According to the sequence of coding these images, Look Up Table is the best way to keep tracking the constantly variation of the translation and/or rotation upon the original 44 slices of CT scan matrix.

5.3.2 Treatment Stage

One image from original CT data matrix has been picked up randomly to undergo the translation and rotation randomly within the same range of variable quantity. As long as the treatment image has been generated, we name it "original", its sinogram and reconstructed images are take their places too as the onsite images we have in radiosurgery treatment. Also, changing all the treatment stage's data format into uint8 is playing important role to mapping the maximum mutual information.

In the comparison process, the "original" is mapping with "1st step matrixes", the sinogram of "original" is mapping with "sinogram matrixes" and the reconstruction image of "original" is mapping with "reconstruction matrixes".

It is no doubt that at a particular scanning angle, there must have three mutual information value maps after the coding and the size of these three maps is 44*275. Finding the maximum mutual information by meshing of these maps or coding by MATLAB function "find" are both useful ways. The following figure shows these three maps at the 3° scanning angle. The maximum mutual information's location is at row = 41 and column = 266.
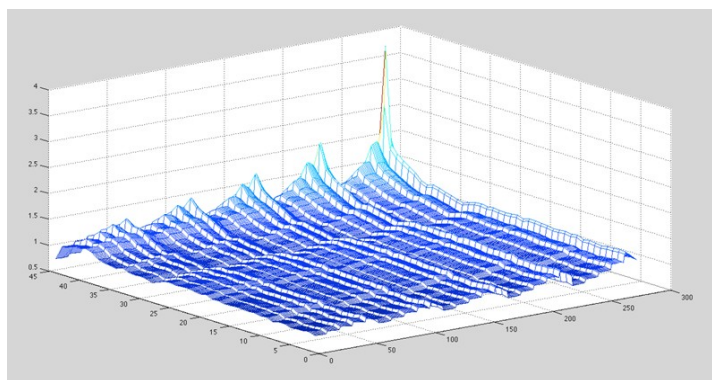
Figure 5.12: MI map of "original" and "1st step matrixes". The maximum value of MI is occurred at the location (41,266).
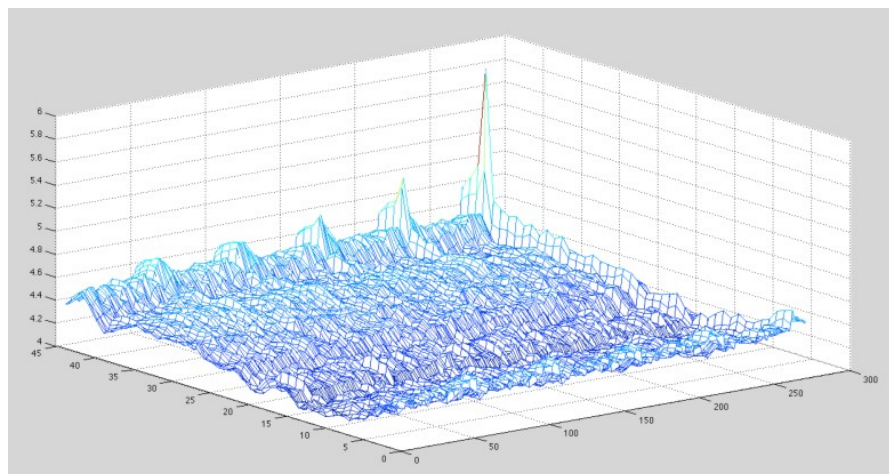
Figure 5.13: MI map of sinogram and "sinogram matrixes". The maximum value of MI is occurred at the location (41,266).

Figure 5.14: MI map of reconstructed image and "reconstruction matrixes". The maximum value of MI is occurred at the location (41,266).

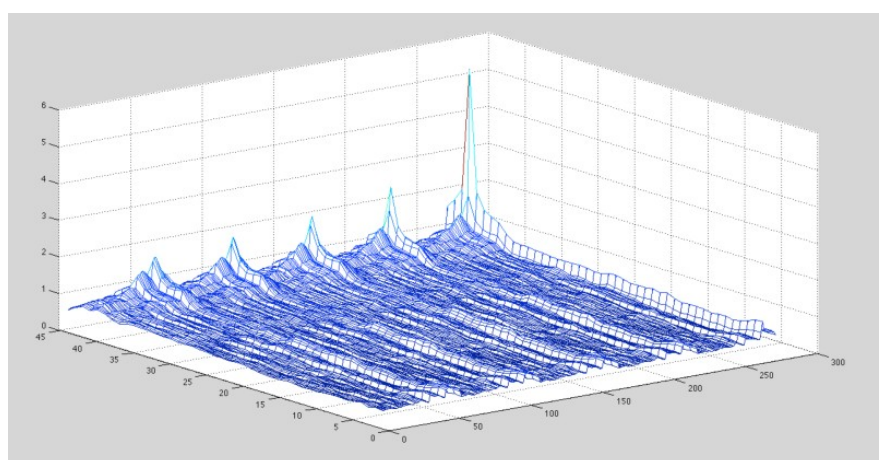Corresponding with the maximum mutual information's column location 266 and row location 41, LUT table shows the patient's shift is 5mm to the right and 5mm to the downward, rotation is 4° clockwise, "original" image is the No.41 slice from the original CT scan matrixes.

258	10 pixels down,5 pixels right, 1 degree clockwise	5mm down, 2.5mm right, 1 degrees clockwi...
259	10 pixels down,5 pixels right	5mm down, 2.5mm right
260	10 pixels down,5 pixels right, 1 degree anticlock...	5mm down, 2.5mm right, 1 degrees anticloc...
261	10 pixels down,5 pixels right, 2 degrees anticlock...	5mm down, 2.5mm right, 2 degrees anticloc...
262	10 pixels down,5 pixels right, 3 degrees anticlock...	5mm down, 2.5mm right, 3 degrees anticloc...
263	10 pixels down,5 pixels right, 4 degrees anticlock...	5mm down, 2.5mm right, 4 degrees anticloc...
264	10 pixels down,5 pixels right, 5 degrees anticlock...	5mm down, 2.5mm right, 5 degrees anticloc...
265	10 pixels down,10 pixels right, 5 degrees clockw...	5mm down, 5mm right, 5 degrees clockwise
266	10 pixels down,10 pixels right, 4 degrees clockw...	5mm down, 5mm right, 4 degrees clockwise
267	10 pixels down,10 pixels right, 3 degrees clockw...	5mm down, 5mm right, 3 degrees clockwise
268	10 pixels down,10 pixels right, 2 degrees clockw...	5mm down, 5mm right, 2 degrees clockwise
269	10 pixels down,10 pixels right, 1 degree clockwise	5mm down, 5mm right, 1 degrees clockwise

Figure 5.15: LUP shows the patient's shift is 10 pixels downward, 10 pixels to the right and 4° clockwise rotated in image domain; In real space, the patient's shift is 5mm to the right and 5mm to the downward, rotation is 4° clockwise.

As we explained in the above two experiments, the record in the MATLAB coding archive indicates the authentic random variables which are automatically chosen by computer. The record in this experiment shows that the random image is No.41 image from the original matrixes and random translations are 5mm to the right and 5mm to the downward, rotation is -4°.

5.3.3 Results and Conclusion

This experiment is provided with sufficient data set and accurate results to demonstrate that mapping partial CT images with the method of mutual information is an efficient way to find the most similar images. The successful matches of partial CT projection and reconstruction images explain that mutual information method in image registration is viable and reliable even though the information is limited within these images. The validity of this design has been proved.

Chapter 6 Conclusion and Future Works

6.1 Conclusion

The first Chapter of this thesis elaborates the development and application of stereotactic radiosurgery system including Gamma-knife, Linear accelerator (LINAC) and LINAC based CyberKnife system, which is the model we used to implement our experiments. Image-guided radiation therapy are also reviewed in this Chapter because our hypothesis and experiments are all around the field of image-guidance system In the following Chapter 2, we fully review the robotic frameless CyberKnife system based on LINAC system specifically in the field of 2D/3D image registration. Hardware and software serving in the current CyberKnife system are explained and recent 2D/3D image registration methods are studied. With the help of 2D/3D registration methods, surgical robots may be programmed by using a preoperative 3D dataset library and a set of intraoperative fluoroscopic or on-site X-ray projections.

In the first section of Chapter 3, we review the CT scan and digitally reconstructed radiographs derived from the pretreatment CT data set. DRR are prepared prior for comparing with the intraoperative X-ray image pairs to help the alignment of patient's on-site position. The second section is all about the mutual information registration method in theory and in applying to the field of image registration. Some animations of simulating CT scan projection and reconstruction process generated by Macromedia Flash are presented in this Chapter.

We raise our hypotheses in Chapter 4: Can we utilize one X-ray camera and the paired detector to simulate partial CT scan to obtain patient's 3D on-site images instead of using two pairs of X-ray imagers to get the X-ray projection images? Can we use these on-site partial CT images to register patient's intraoperative position by mutual information image-registration method? What is the result if we apply a very small angle in the partial CT scanning angle? Based on these questions, our designs present in the end of this Chapter in order to simplify the image-guided system of CyberKnife system that the image-guided system may be fulfilled by a narrow-angle-movable robotic couch and one X-ray camera fixing on the ceiling to capture the patient's intraoperative partial CT projection images, along with the image registration processing by mutual information method.

Three experiments demonstrate in Chapter 5 in sequence: the first experiment is for proving the validity of mutual information by contrasting the alignment result using mutual information with the alignment result using two orthogonal X-ray stereotactic imagers; we proposed in Chapter 4 that partial CT may be an approach for simplifying image registration by mapping maximum mutual information, therefore the second experiment is about calculating the maximum mutual information between reconstructed partial CT images; the last experiment is built to prove that our design is theoretically feasible to simplify onsite image registration approach for radiosurgery by partial CT. The abundant results from these three experiments can explain the validity and the implement ability of our partial CT design combined with mutual information method.

6.2 Future Works

1) Error analysis: we cannot finish the error analysis job in this thesis because of the huge dataset take us a lot of time to conduct. In the future, we are going to do the error analysis of the value of mutual information between partial CT reconstructed images and partial CT sonograms; between wider partial CT scanning angles and narrower partial CT scanning angles; between partial CT reconstructed images and X-ray stereotactic image pairs, etc.. Calculating the accuracy of our design will play an important part in our future studies.

2) So far, our last experiment is on 4D only because the limitation of the time. However, the real simulation should go 6D for any rigid subject. In next studies, we are going to simulate 6D translation and rotation: x, y, z, yaw, pitch and roll, as the patient's real displacement during radiosurgery treatment. These variable quantities in 6D should be more accurate with smaller variations. Also, the accuracy is the indispensable indicator in the next studies.

3) Graphical User Interface (GUI) is a best way to build an interface that allows users to interact with our experiments by using images of result. The goal of our GUI is to help users to understand and verify our experiments by choosing their own combination of patient's intraoperative position through GUI interface and can observe the result compares with their own input data.

Appendix

Simulation process of MATLB coding

Ray Casting

DETERMINE	the target matrix
INITIAL	row is the row number of matrix
	column is the column number of matrix
	dimension is the image number of matrix
INITIAL	define two arrays as the projection image pairs

FOR   every image in matrix
        FOR   rotate this image with 45°;
                sum intensities in every column of image in the new coordinates;
                locate the every slice of the summation of intensity to the
                corresponding column in one projection image.

                rotate this image with -45°;
                sum intensities in every column of image in the new coordinates;
                locate the every slice of the summation of intensity to the
                corresponding column in another projection image.
        END
END

Mapping of intensity range from 16 bit to 8 bit

DETERMINE the target matrix
INITIAL   row is the row number of matrix
       column is the column number of matrix
       dimension is the image number of matrix
INITIAL   find the maximum intensity value of matrix
       find the minimum intensity value of matrix

FOR every image in matrix
    FOR every row in this image;
       FOR every column in this image;
         find the intensity value of the pixel located in image(row, column);
         new intensity value in the range of 8 bit equals to

$$\frac{\text{intensity value in image(row, column)} - \text{minimum intensity value of matrix}}{\text{maximum intensity value of matrix} - \text{minimum intensity value of matrix}} * 2^8$$

         put the new intensity value back to the pixel located in
         image (row, column)
         END
    END
END

References

1. American Society for Radiation Oncology(ASTRO) Stereotactic radiosurgery (SRS) model coverage policy (http://www.astro.org) . ASTRO website, 2010.

2. Anil, S. M., Tetsuo, K., Yoko, K., Shinya, N., & Hirotoshi, S. An overview in stereotactic radiosurgery. *Pan ARAB Journal of Neurosurgery*.2009, April; volume 13, No.1.

3. Liu, C. Y., & Apuzzo, M. L. (2003). The genesis of neurosurgery and the evolution of the neurosurgical operative environment: Part I-Prehistory to 2003. *Neurosurgery*, 52(1), 3-19.

4. Goetsch, S.J. Linear accelerator and gamma knife-based stereotactic cranial radiosurgery: challenges and successes of existing quality assurance guidelines and paradigms. *International Journal of Radiation Oncology, Biology, Physics*.2008; 71(1 Suppl):S118-21.

5. Leksell, L. The stereotaxic method and radiosurgery of the brain. *Acta Chir. Scand*. 1951;102(4):316-9.

6. de Lunsford, D. L., Flickinger, J., Lindner, G., & Maitz, A. (1989). Stereotactic radiosurgery of the brain using the first United States 201 cobalt-60 source gamma knife. *Neurosurgery*, 24(2), 151-159.

7. RadiologyInfo Stereotactic Radiosurgery (http://www.radiologyinfo.org/). RadiologyInfo.org website. 2012, July.

8. Verellen, D., De Ridder, M., Linthout, N., Tournel, K., Soete, G., & Storme,G. (2007). Innovations in image-guided radiotherapy. *Nature Reviews Cancer*, 7(12), 949-960.

9. Timmerman, R.D., & Xing, L. (2009). In Image-guided and Adaptive Radiation Therapy. Lippincott Williams & Wilkins, 2009; pp 16-37.

10. Peters, T.M., & Cleary, K.R. (2008). In Image-guided Interventions: Technology and Applications. Springer, 2008; pp 1-13.

11. Chang, S. D., Main, W., Martin, D. P., Gibbs, I. C., & Heilbrun, M. P. (2003). An analysis of the accuracy of the CyberKnife: a robotic frameless stereotactic radiosurgical system. *Neurosurgery*, 52(1), 140-147.

12. Friehs, G.M., Park, M.C., Goldman, M.A., et al. Stereotactic radiosurgery for functional disorders. *Neurosurgical Focus*, 2007; 23(6):E3.

13. Pannullo, S. C., Yama, C., & Wernicke, A. G. Stereotactic radiosurgery for brain tumors. Diagnostic Techniques and Surgical Management of Brain Tumors. *InTech*, 2011. 434-446.

14. Adler, J. R., Jr., Chang S. D., Murphy M. J., Doty J., Geis P., Hancock S. L., The Cyberknife: a frameless robotic system for radiosurgery. *Funct Neurosurg* 69, 124-128 (1997).

15. Adler, J. R., Schweikard, A., Murphy, M. J., Hancock, S. L. Image-guided cyberknife radiosurgery. In: Barnett, G., Roberts, D., Maciunas, R. J. (eds) Image-Guided Neurosurgery: Clinical Applications of Interactive Surgical Navigation, edn. Quality Medical Publishing, pp 193-204 (1998).

16. Adler, J. R., Jr., Murphy, M. J., Chang, S. D., Hancock, S. L. Image-guided robotic radiosurgery. *Neurosurgery* 44, 1299-1306; discussion 1306-1297 (1999).

17. Murphy, M. J., Cox, R. S. The accuracy of dose localization for an image-guided frameless radiosurgery system. *Med Phys* 23, 2043-2049 (1996).

18. Murphy, M. J. An automatic six-degree-of-freedom image registration algorithm for image-guided frameless stereotaxic radiosurgery. *Med Phys* 24, 851-866(1997).

19. Schweikard, A., Bodduluri, M., Adler, J. R. Planning for camera-guided robotic radiosurgery. *IEEE Transactions on Robotics and Automation* 14, 951-962 (1998).

20. Kilby, W., Dooley, J. R., Kuduvalli, G., Sayeh, S., & Maurer Jr, C. R. (2010). The CyberKnife robotic radiosurgery system in 2010. *Technol Cancer Res Treat*, 9(5), 433-52.

21. Hara, W., Soltys, S. G., & Gibbs, I. C. (2007). CyberKnife® Robotic Radiosurgery system for tumor treatment. *Expert Review of Anticancer Therapy*, 7(11), 1507-1515.

22. Brown, W.T., et al. CyberKnife® radiosurgery for stage I lung cancer: results at 36 months. *Clinical Lung Cancer* 8.8 (2007): pp 488-492.

23. Adler, J. R., Jr., Bower, R., Gupta, G., Lim, M., Efron, A., Gibbs, I. C., Chang, S. D., Soltys, S. G. Nonisocentric radiosurgical rhizotomy for trigeminal neuralgia. *Neurosurgery* 64, A84-90 (2009).

24. Colombo, F., Casentini, L., Cavedon, C., Scalchi, P., Cora, S.,Francescon, P. Cyberknife radiosurgery for benign meningiomas: short-term results in 199 patients. *Neurosurgery* 64, A7-13 (2009).

25. Colombo, F., et al. Early results of CyberKnife radiosurgery for arteriovenous malformations. *Journal of Neurosurgery* 111.4 (2009): 807-819.

26. Soltys, S. G., Adler, J. R., Lipani, J. D., Jackson, P. S., Choi, C. Y.,Puataweepong, P., White, S., Gibbs, I. C., Chang, S. D. Stereotactic radiosurgery of the postoperative resection cavity for brain metastases. *Int J Radiat Oncol Biol Phys* 70, 187-193 (2008).

27. Wowra, B., Muacevic, A., Tonn, J. C. Quality of radiosurgery for single brain metastases with respect to treatment technology: a matched-pair analysis. *J Neurooncol* 94, 69-77 (2009).

28. Chang, S. D., Jr., Adler, J. R., Jr. CyberKnife radiosurgery for benign intradural extramedullary spinal tumors. *Neurosurgery* 58, 674-685; discussion 674-685 (2006).

29. Gagnon, G. J., Nasr., N. M., Liao, J. J., Molzahn, I., Marsh, D., McRae,D., Henderson, F. C., Sr. Treatment of spinal tumors using cyberknife fractionated stereotactic radiosurgery: pain and quality-of-life assessment after treatment in 200 patients. *Neurosurgery* 64, 297-306; discussion 306-297 (2009).

30. Gibbs, I. C. Spinal and paraspinal lesions: the role of stereotactic body radiotherapy. *Front Radiat Ther Oncol* 40, 407-414 (2007).

31. Sahgal, A., Ames, C., Chou, D., Ma, L., Huang, K., Xu, W., Chin, C., Weinberg, V., Chuang, C., Weinstein, P., Larson, D. A. Stereotactic body radiotherapy is effective salvage therapy for patients with prior radiation of spinal metastases. *Int J Radiat Oncol Biol Phys* 74, 723-731 (2009).

32. Sinclair, J., Chang, S. D., Gibbs. I. C., Adler, J. R., Jr. Multisession. CyberKnife radiosurgery for intramedullary spinal cord arteriovenous malformations. *Neurosurgery* 58, 1081-1089; discussion 1081-1089 (2006).

33. Gerszten, P. C., Burton, S. A., Ozhasoglu, C., Welch, W. C. Radiosurgery for spinal metastases: clinical experience in 500 cases from a single institution. *Spine* 32, 193-199 (2007).

34. Collins, B. T., Vahdat, S., Erickson, K., Collins, S. P., Suy, S., Yu, X., Zhang, Y., Subramaniam, D., Reichner, C. A., Sarikaya, I., Esposito, G., Yousefi, S., Jamis-Dow, C., Banovac, F., Anderson, E. D. Radical cyberknife radiosurgery with tumor tracking: an effective treatment for inoperable small peripheral stage I non-small cell lung cancer. *J Hematol Oncol* 2, 1 (2009).

35. Coon, D., Gokhale, A. S., Burton, S. A., Heron, D. E., Ozhasoglu, C.,& Chrisite, N. Fractionated stereotactic body radiation therapy in the treatment of primary, recurrent, and metastatic lung tumors: the role of positron emission tomography/computed tomography-based treatment planning. *Clin Lung Cancer* 9, 217-221 (2008).

36. King, C. R., Brooks, J. D., Gill, H., Pawlicki, T., Cotrutz, C., Presti, J. C.,Jr. Stereotactic body radiotherapy for localized prostate cancer: interim results of a prospective phase II clinical trial. *Int J Radiat Oncol Biol Phys* 73, 1043-1048 (2009).

37. Choi, B. O., Choi, I. B., Jang, H. S., Kang, Y. N., Jang, J. S., Bae, S. H, Yoon, S. K., Chai, G. Y., Kang, K. M. Stereotactic body radiation therapy with or without transarterial chemoembolization for patients with primary hepatocellular carcinoma: preliminary analysis. *BMC Cancer* 8, 351 (2008).

38. Knaan, D., & Joskowicz, L. Effective intensity-based 2D/3D rigid registration between fluoroscopic X-ray and CT. Lecture Notes on Computer Science, 2878(1):351–358, 2003.

39. Zitova, B., & Flusser, J.(2003). Image registration methods: a survey. *Image and Vision Computing,21* (2003); pp. 977-1000.

40. Penney, G. P., Weese, J., Little, J. A., Desmedt, P., & Hill, D. L. G. (1998). A comparison of similarity measures for use in 2-D-3-D medical image registration. *Medical Imaging, IEEE Transactions on, 17*(4): pp. 586-595.

41. Metz, C. T., and Nucletron bv Veenendaal. Digitally reconstructed radiographs. Diss. Master thesis, Utrecht University, 2005.

42. Dorgham, O., M. Fisher, and S. Laycock. Performance of a 2D-3D image registration system using (lossy) compressed x-ray CT. *Annals of the BMVA* 2009.3 (2009): 1-11.

43. Goldman, L. W. (2007). Principles of CT and CT technology. *Journal of Nuclear Medicine Technology*, 35(3); 115-128.

44. Pettersson, H.,Allison D.,& Schulthess, G. K. (1998).The Encyclopaedia of Medical Imaging Vol 1: Physics, Techniques and Procedures. Informa Healthcare; 1 edition (November 1998); 95-96.

45. Kak, A. C., & Slaney, M. (1987). Algorithms for reconstruction with nondiffracting sources. Principles of Computerized Tomographic Imaging. The Institute of Electrical and Electronics Engineers, Inc.; pp. 49-112; Chapter 3.

46. Wei, S. (2005). Recent development on computer aided tissue engineering. *Journal of Medical Biomechanics*, 20(3); 179-192.

47. Studholme, C., Hill, D. L., & Hawkes, D. J. (1996). Automated 3-D registration of MR and CT images of the head. *Medical Image Analysis, 1*(2), 163.

48. Maes, F., Vandermeulen, D., & Suetens, P. (2003). Medical image registration using mutual information. *Proceedings of the IEEE, 91*(10), 1699-1722.

49. Cover, T. M., & Thomas, J. A. (2006). Elements of information theory, 2nd edition. Wiley-Interscience, July 18, 2006; pp. 12-49; Chapter 2.

50. Latham, P. E., & Roudi, E. (2009). Mutual information (www.scholarpedia.org). Scholarpecia website, 4(1):1658.

51. Jacquet, W. Focus Mutual Information for Medical Image Alignment in Dentistry, Orthodontics and Craniofacial Surgery. (2010). Academic & Scientific Publishers, September 1, 2010; pp. 29-44; Chapter 3.

52. Maes, F., Collignon, A., Vandermeulen, D., Marchal, G., & Suetens, P. (1997). Multimodality image registration by maximization of mutual information. *Medical Imaging, IEEE Transactions on, 16*(2), 187-198.

53. Weisstein, E. W. Radon transform (http://mathworld.wolfram.com). MathWorld--A Wolfram Web Resource.

54. Poularikas, A. D. Transforms and Applications Handbook, Third Edition (2010). CRC Press, January 19, 2010; Chapter 8.

55. Radon Transform (http://www.mathworks.com). MathWorks website, 2012.

56. MATLAB Overview (http://www.mathworks.com). MathWorks website, 2012.